

 M 2017

**U.** PORTO

**FEUP** FACULDADE DE ENGENHARIA  
UNIVERSIDADE DO PORTO

 **Fraunhofer**  
IWS

# **Zinc Oxide Coatings for Thermoelectric Applications via Thermal Spray**

**Gonçalo Cristóvão dos Santos Queirós**

MASTER THESIS DISSERTATION

Mestrado Integrado em Engenharia Metalúrgica e de Materiais

Internal Supervisor: Elsa Wellenkamp Sequeiros, Dr.-Ing

External Supervisor: Maria Barbosa, Dr.-Ing

July 31, 2017



# **Zinc Oxide Coatings for Thermoelectric Applications via Thermal Spray**

**Gonçalo Cristóvão dos Santos Queirós**

Mestrado Integrado em Engenharia Metalúrgica e de  
Materiais

July 31, 2017

# Acknowledgements

Gostaria de expressar minha sincera gratidão à minha orientadora acadêmica, Elsa Sequeiros, por todo o apoio e orientação. A sua paciência e capacidade para exemplificar tudo até ao mais pequeno pormenor, foi sem dúvida uma grande ajuda ao longo deste trabalho.

Um especial obrigado à minha orientadora de estágio, Maria Barbosa, por toda a energia e mais alguma, mas toda ela positiva. Tudo se torna mais fácil ao trabalhar com alguém com um conhecimento tão amplo, e com capacidade de me motivar a trabalhar mais e a ser melhor.

A special thanks goes out to all the members of Fraunhofer IWS, for accepting me and letting me be a small part of the company during my journey. Fraunhofer IWS institute provided me the funding for my work, technical support and material. This research would not have been possible without them.

Por último, e talvez mais importante, um obrigado muito especial à minha família e amigos: são tudo o que é preciso para tornar minha vida digna de ser vivida. Aos meus pais, que sempre me ajudaram a realizar todos os meus sonhos, e que sem eles nada disto seria possível. Ao António Silva, que me acompanhou pela segunda vez nesta jornada internacional (mais aventuras virão!). Gostaria de agradecer também à minha namorada, Sofia Silveira, pela sua enorme paciência em aguentar as minhas divagações e crises existenciais, e também pela a grande ajuda no desenvolvimento desta tese.

*“Everything seems impossible, until it’s done”*

Nelson Mandela

# Resumo

A investigação eficiente de fontes de energia é um dos maiores desafios da atualidade. Estima-se que mais de 60% da energia consumida seja gasta em vão, a maioria sob a forma de calor. No entanto, esse calor pode ser diretamente convertido em eletricidade, utilizando geradores termoelétricos (TEG). Embora vários materiais tenham demonstrado ter ótimas propriedades termolétricas, a aplicação dos mesmos é limitada devido à sua toxicidade, disponibilidade e custos de processamento e exploração relativamente elevados. O óxido de zinco (ZnO) é um material termoelétrico (TE) bastante promissor. Normalmente, os materiais termoelétricos baseados em ZnO são produzidos por diversas técnicas, tais como a evaporação térmica, deposição química em fase de vapor (CVD), pirólise de pulverização, deposição física em fase vapor (PVD) e revestimento sol-gel-dip. Essas técnicas são bastante caras ou demoradas. No entanto, o thermal spray permite a deposição de um revestimento multicamadas com uma única tecnologia. Além disso, traz flexibilidade relativamente à forma e à geometria devido à possibilidade de depositar o gerador termoelétrico (TEG) diretamente na fonte de calor.

A componente prática desta dissertação foi focada na produção de revestimentos densos de ZnO, através de atmospheric plasma spray (APS). De início, como material de alimentação, foi utilizado um pó de ZnO comercialmente disponível. Após a otimização do processo APS, os respectivos parâmetros foram ajustados de forma a depositar a partir de uma suspensão (processo S-APS) com base no pó de ZnO previamente depositado.

A influência da corrente, distância de pulverização e composição de gás foi estudada no processo de deposição APS, utilizando quer pó, quer suspensão de ZnO. De forma a obter revestimentos de maior espessura, as partículas devem adquirir grandes quantidades de energia térmica e cinética. Verificou-se então que os revestimentos mais espessos foram obtidos utilizando correntes elevadas e grandes quantidades de H<sub>2</sub>. Por outro lado, a percentagem de Ar e a distância do spray têm um efeito negativo sobre a espessura do revestimento. Na experiência APS, APS22 foi a melhor condição de deposição, onde foi obtido um revestimento de 140 µm de espessura. No entanto, no caso do S-APS, a melhor condição foi o S-APS1, que resultou em um revestimento de 170 µm de espessura. É possível também observar que a utilização de suspensões permitiu obter revestimentos com melhor qualidade e que devido à continuidade do processo é uma técnica vantajosa para a aplicação industrial. Apesar de ser necessária a otimização do processo, os resultados são bastante promissores.

# Abstract

The efficient exploration of energy sources is one of today's biggest challenges. It is estimated that more than 60% of the consumed energy is lost in vain, most of it in the form of heat. However, heat can be directly converted into electricity by using thermoelectric generators (TEG). Although several materials have been shown to have great thermoelectric performance, their application is limited due to their toxicity, availability and relatively high processing and exploration costs. Zinc oxide (ZnO) is a well-established thermoelectric (TE) material. Normally ZnO based TE materials are produced by many techniques, such as thermal evaporation (PVD), chemical vapor deposition (CVD), spray pyrolysis, physical vapor deposition and sol-gel-dip-coating. These techniques are quite expensive or time-consuming. However, thermal spray allows for the deposition of a multi-layered coating with one single technology. Moreover, it brings flexibility in form and geometry due to the possibility of depositing the TEG directly on the heat source.

The practical component of this dissertation focused on the production and dense coatings of ZnO via atmospheric plasma spray (APS). At the beginning, as feedstock material, commercially available ZnO powder was used. After optimization of the APS process, its parameters were adjusted to deposit from a suspension (S-APS process) based on the previously deposited ZnO powder.

The influence of current, spray distance and gas composition was studied in both powder and suspension APS deposition. In order to obtain thicker coatings, particles should acquire large amounts of both thermal and kinetic energy. It was then verified that thicker coatings are obtained using high currents and large H<sub>2</sub> amounts. On the other hand, Ar content and spray distance have a negative effect on the coating thickness. In APS experiment, APS22 was the best condition of deposition, where a coating of 140 μm thickness was obtained. However, in the case of S-APS, the best condition was S-APS1, which resulted in a coating of 170 μm thickness. It is also possible to observe that the use of suspensions allowed to obtain coatings with better quality and that due to the continuity of the process is an advantageous technique for the industrial application. Although optimization of the process is required, the results are quite promising.

# Contents

<b>1</b>	<b>Motivation</b>	<b>1</b>
<b>2</b>	<b>Literature Review</b>	<b>4</b>
2.1	Fundamentals of Thermoelectrics . . . . .	4
2.1.1	State-of-the-art: Materials . . . . .	6
2.1.2	State-of-the-art: Manufacturing Processes . . . . .	8
2.2	Zinc Oxide (ZnO) . . . . .	9
2.2.1	Basic properties and applications . . . . .	9
2.2.2	Processing . . . . .	13
2.3	Thermal Spray . . . . .	13
2.3.1	Atmospheric plasma spray . . . . .	15
2.3.1.1	Process variables . . . . .	16
2.3.1.2	Feedstock material . . . . .	19
<b>3</b>	<b>Experimental Procedure</b>	<b>22</b>
3.1	Materials . . . . .	22
3.1.1	Powder . . . . .	22
3.1.2	Suspension . . . . .	22
3.1.3	Substrate . . . . .	23
3.2	Coating process . . . . .	23
3.2.1	Design of Experiments - APS . . . . .	23
3.2.2	Design of experiments - S-APS . . . . .	27
3.3	Coating characterization . . . . .	29
3.3.1	Thickness measurement . . . . .	29
3.3.2	Metallographic preparation for optical and electron microscopy analysis . . . . .	30
3.3.3	OM and SEM analysis . . . . .	30
3.3.4	Chemical composition . . . . .	31
3.3.5	Mechanical properties . . . . .	31
<b>4</b>	<b>Results and Discussion</b>	<b>32</b>
4.1	Material characterization . . . . .	32
4.1.1	Powder . . . . .	32
4.1.2	Suspension . . . . .	33
4.2	APS coatings Characterization . . . . .	34
4.2.1	Thickness measurement . . . . .	34

4.2.2	Hardness measurement . . . . .	39
4.3	S-APS coating characterization . . . . .	40
4.3.1	Thickness measurement . . . . .	40
4.3.2	Hardness measurement . . . . .	45
4.4	Powder vs Suspension deposition . . . . .	45
4.4.1	Coating stability in air . . . . .	45
4.4.2	Coating morphology . . . . .	46
4.4.3	Chemical composition . . . . .	48
4.4.4	Mechanical properties . . . . .	50
<b>5</b>	<b>Conclusions and future work</b>	<b>52</b>
1	XRD analysis with indexed phases . . . . .	55
	<b>References</b>	<b>56</b>

# List of Figures

1.1	Schematic representation of the amount of primary energy converted into consumable energy, and their loss in the form of heat . . . . .	1
2.1	Thermoelectric device and thermoelectric cell . . . . .	4
2.2	Optimization of ZT through carrier concentration tuning . . . . .	6
2.3	A schematic of the wurtzite ZnO crystal structure . . . . .	10
2.4	Schematic illustration of thermal spray APS . . . . .	14
2.5	Schematization of relationship between thermal and kinetic energy for the different TS processes . . . . .	15
2.6	Schematization of a plasma equipment . . . . .	16
2.7	Concepts of critical velocity . . . . .	17
2.8	The droplet/particle temperature and trajectory in suspension plasma spray at different standoff distances (D) . . . . .	17
2.9	APS and HVOF suspension thermal spray injectors . . . . .	19
2.10	Three-vessels suspension feeder (Fraunhofer IWS) . . . . .	20
2.11	Schematization of a suspension feeding system with integrated agitator three-vessels . . . . .	20
3.1	Fischer Dualscope equipment and respective working principle . . . . .	29
4.1	ZnO particle size distribution . . . . .	32
4.2	SEM images of the surface of ZnO powder . . . . .	33
4.3	SEM images of ZnO powder and respective EDS analysis . . . . .	33
4.4	ZnO suspension particle size distribution . . . . .	34
4.5	Influence of variable spray parameters in coating thickness . . . . .	36
4.6	Interaction between APS variable spray parameters in coating thickness . . . . .	36
4.7	OM images of samples APS10 and APS20 . . . . .	38
4.8	OM images of samples APS19 and APS22 . . . . .	39
4.9	Vickers Hardness measurement of APS coatings . . . . .	40
4.10	Main effect of the variable spray parameters in coating thickness . . . . .	41
4.11	Interaction between S-APS variable spray parameters in coating thickness . . . . .	42
4.12	Pareto chart of effects . . . . .	43
4.13	SEM images of S-APS 1 and S-APS 7 coatings . . . . .	43
4.14	SEM images of S-APS 3 and S-APS 4 coatings . . . . .	44
4.15	Vickers Hardness measurement of S-APS coatings . . . . .	45
4.16	Surface image of APS22, S-APS1 and S-APS2 . . . . .	46

4.17 SEM images of APS22 surface . . . . .	47
4.18 SEM images of S-APS1 surface . . . . .	47
4.19 SEM images of S-APS2 surface . . . . .	48
4.20 XRD analysis of APS22, S-APS1 and S-APS2 samples . . . . .	48
4.21 SEM images of S-APS1 cross section . . . . .	49
4.22 EDS spectrum of Z1 (marked in Figure 4.21) . . . . .	50
4.23 Vickers Hardness measurement (HV 0.3) of APS22 and S-APS1 . . . . .	51

# List of Tables

2.1	State-of-the-art materials used for TE applications . . . . .	8
2.2	Previous studies on doping of ZnO TE materials . . . . .	12
2.3	Plasma gas comparison . . . . .	18
3.1	Fixed spray parameters for APS DoE . . . . .	24
3.2	Matrix of experiments of APS coatings . . . . .	24
3.3	Variable parameters for APS DoE . . . . .	25
3.4	Matrix of interactions . . . . .	26
3.5	Fixed spray parameters for S-APS DoE . . . . .	27
3.6	Matrix of experiments of S-APS . . . . .	28
3.7	Variable parameters for S-APS DoE . . . . .	28
3.8	Matrix of interactions of S-APS . . . . .	29
4.1	ZnO suspension characteristics . . . . .	34
4.2	Thickness and deposition per pass results from APS deposition . . . . .	35
4.3	Variable parameters for additional APS experience . . . . .	37
4.4	Suspension deposition parameters and and respective thickness measurement . . . . .	41
4.5	Suspension deposition center point parameters and respective thickness measurement . . . . .	41

# Abbreviations

(a&s)	agglomerated and sintered
AC	Arc current
AIST	National Institute of Advance Science and Technology
APS	Atmospheric plasma spray
CAPS	Controlled atmosphere plasma spray
CEMUP	Centro de Materiais da Universidade do Porto
CVD	Chemical vapor deposition
DC	Continuous current
DLR	German aerospace center
DoE	Design of experiments
EDS	Energy dispersive X-ray spectroscopy
GP	Gas pressure sintering
HIP	Hot isostatic pressing
HP	Hot pressing
HVAF	High velocity air-fuel
HVOF	High velocity oxy-fuel
OM	Optical microscopy
PS	Plasma spray
PVD	Physical vapor deposition
S-APS	Suspension atmospheric plasma spray
SD	Spray distance
SEM	Scanning electron microscope
SPS	Spark plasma sintering
TE	Thermoelectric
TEG	Thermoelectric generator
TS	Thermal spray
XRD	X-ray powder diffraction
ZT	Figure of merit

# Chapter 1

## Motivation

Worldwide the demand for energy is continuously growing, and, according to the forecasts of the International Energy Agency, it is expected to rise by approximately 50 % until 2030 [1]. At the same time, also the awareness for global environmental prevention is increasing. This requires smart solutions, such as the development of new technologies for energy conversion, storage and transmission [1–3].

It is estimated that, more than 60% of the consumed energy is lost in vain, most of it in the form of heat (Figure 1.1) [4, 5]. One valuable approach to improve the overall energy efficiency consists in capturing and re-using this waste heat, which is intrinsic not only to all industrial manufacturing processes, but also to many daily utilities (transports, co-generation systems, household supplies, etc.). There are several available technologies which make profit of this produced heat, such as recuperators, waste heat boilers and thermoelectric generators (TEGs), giving it a productive end-use [3, 6, 7].

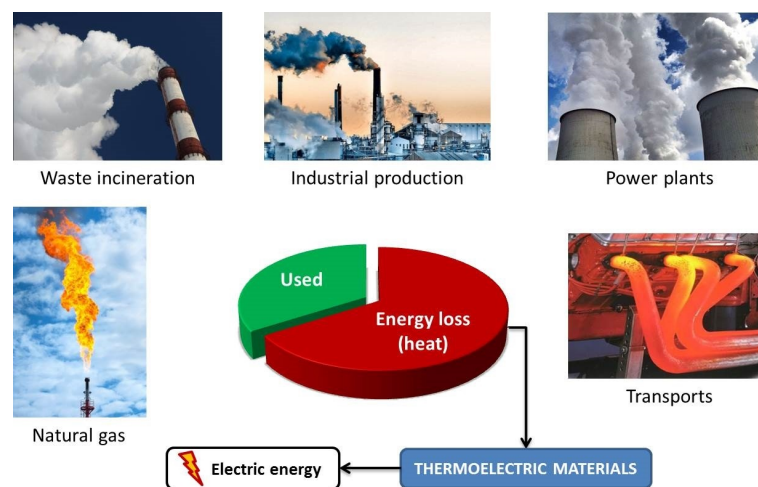


Figure 1.1: Schematic representation of the amount of primary energy converted into consumable energy, and their loss in the form of heat

Thermoelectric generators are particularly interesting due to the possibility of directly convert the waste heat into electricity (one-step process), while other alternatives often need to create first mechanical energy which will later drive an electrical generator (two-step-process) [3, 7, 8].

It has been demonstrated that thermal spraying (TS) has the potential to be a cost effective alternative process for the production of large area thermoelectric (TE) materials [3, 4]. Due to the flexibility of TS processes, several variables can be adjusted in order to deposit a multilayer system containing all different materials that are required for a TEG. The interest of TS is also based on its high deposition rates and the possibility to coat a wide range of substrate materials [3, 9].

At literature [10–17] are only reported few materials processed by TS for TE applications since the commercially availability thermoelectric materials are very expensive (such as Bi, Te or Ge) or contain extremely toxic components such as Pb or Sb. The processing of TE by TS has been very limited. In the 90s, both Aachen University of Technology and the German Aerospace Center (DLR) conducted an investigation about  $\beta$ -FeSi<sub>2</sub> deposited by controlled atmosphere plasma spray (CAPS), meeting the condition of being a cheap and non-toxic TE material [10–14]. At around the same time, Co-doped  $\beta$ -FeSi<sub>2</sub> was also a target of investigation in Japan, by the National Institute of Advanced Science and Technology (AIST), which processed this material also with CAPS [4, 15]. A decade later, new interest arises with the deposition of Sr<sub>0.9</sub>Y<sub>0.1</sub>TiO<sub>3</sub>, as a n-type material and a thermally sprayed tubular TEG, also conducted by AIST [16, 17]. In the meantime, Longtin *et al.* [18] studied the deposition of FeSi<sub>2</sub> and Mg<sub>2</sub>Si metal silicide coatings for automotive applications.

More recently, a completely thermally sprayed TEG has been developed at Fraunhofer IWS (Germany), where Ca<sub>2</sub>Fe<sub>2</sub>O<sub>5</sub> (p-type) and TiO<sub>x</sub> (n-type) were used as semiconductors. Although the TEG was functional, the device efficiency was limited mainly due to the electric conductivity of the chosen materials. Alternative TE materials which are able to be processed by TS are highly desirable to establish this technology as an alternative for TEG manufacture [4, 19].

A proper TE material should have specific properties, such as high Seebeck coefficient, high electrical conductivity and low thermal conductivity. Moreover, it should be sprayable, *i.e.* it should melt without decompose and without suffer significant phase transformations. Zinc oxide (ZnO) is a well-established TE material for high temperature applications. It can be doped both as a p-type and n-type semiconductor, and it has high thermal and chemical stability [20–23]. ZnO is currently processed by atmospheric plasma spraying (APS) for the production of sputtering targets (Firma Heraeus) [21].

This thesis is focused on the processing of commercially available ZnO powder by

TS, aiming to obtain dense mechanical stable coatings which will later be optimized for TE applications. Particularly challenging is its high melting temperature (1975 °C) and the risk of zinc dissociation during deposition, not only in terms of properties achieved, but also due to its toxicity.

In order to study the feasibility of this material for the production of TEG's, the first approach of this preliminary research will be the deposition of the standard feedstock powder of ZnO, through atmospheric plasma spray (APS), which process will be parameterized by means of a design of experiments (DoE). For the DoE, the influence of different process variables on the coating properties will be quantified and the process optimized accordingly. After optimization, a suspension with the same composition will be used as feedstock material in order to obtain coatings with higher density.

# Chapter 2

## Literature Review

### 2.1 Fundamentals of Thermoelectrics

Thermoelectric generators are a promising solution to handle the future challenges in the energy sector. They find application in waste-heat recovery, power generation, and solid state cooling [8, 24].

Figure 2.1 shows how a typical TEG is built. It is constituted by several thermoelectric cells (Figure 2.1- right), which consist in n-type (free electrons) and p-type elements (free defect electrons), electrically contacted in series and thermally in parallel [6, 24].

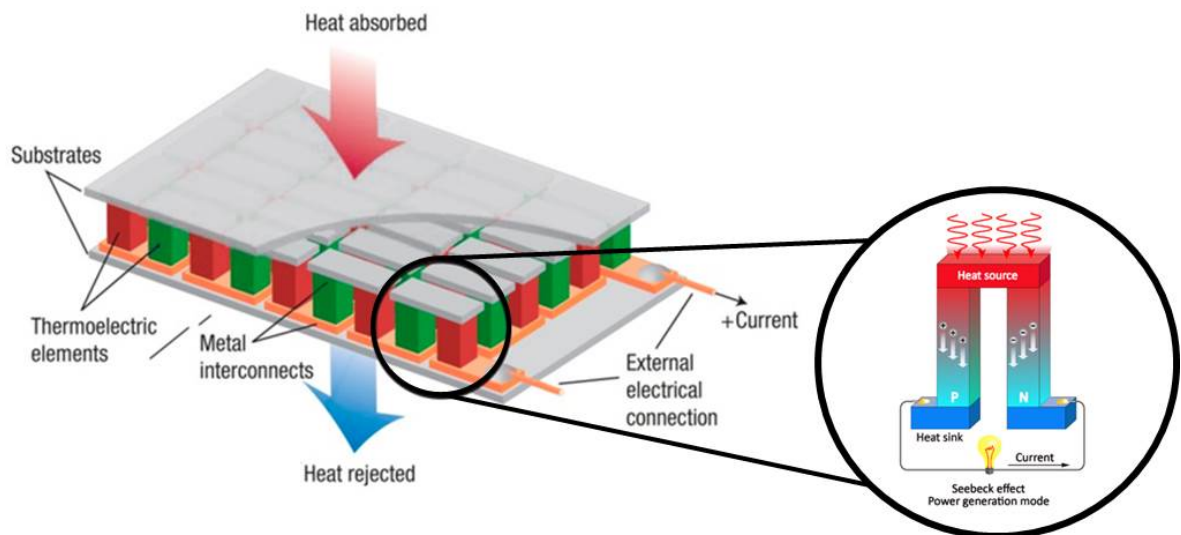


Figure 2.1: A thermoelectric device (left) and a representation of a thermoelectric cell (right) [2, 25]

The source of the thermoelectric effect is the transport of thermal and electric energy in conducting materials. The conversion process of thermal energy into electricity is

called the Seebeck effect. Seebeck first observed that when two dissimilar conducting materials are joined together, and their junctions are held at different temperatures ( $T_1$  and  $T_2$ ), a proportional potential difference is generated ( $\Delta U$ ). The voltage developed to the temperature difference is defined as the Seebeck coefficient or thermopower,  $\alpha$ , with the unit of V/K. In more specific terms, the temperature gradient ( $\Delta T$ ) induces a diffusion of the charge carriers, from the hot-end to the cold-end of the material. Then, by collecting the free carriers on the cold side, an electric voltage is generated. The inverse phenomenon, in which electricity produces a temperature difference, is called the Peltier effect, used in thermoelectric cooling applications, for example in refrigerators [6, 26, 27].

The major challenge in implementing thermoelectric power generation technology is the relatively low energy conversion efficiency [19]. The performance of a TEG depends not just on the power produced but also how much heat is provided at the hot end. It can be shown that the maximum efficiency of a thermoelectric material depends on two terms. The first is the Carnot efficiency, which can not be exceeded in all heat engines. The second is a term that depends on the thermoelectric properties, Seebeck coefficient, electrical resistivity and thermal conductivity [2, 28]. These properties all appear together and thus form a new material property, the Thermoelectric Figure of Merit ( $ZT$ ), given by:

$$ZT = \frac{\alpha^2 \sigma T}{k} = \frac{\alpha^2 T}{\rho k} \quad (1)$$

where  $\alpha$  is the Seebeck coefficient (V/K),  $\sigma$  is the electrical conductivity (S/m),  $\rho$  the electrical resistivity ( $\Omega \cdot m$ ),  $k$  the thermal conductivity (W/m.K) and  $T$  is the temperature (K). Efficient materials have  $ZT$  values near to unity or greater.  $ZT = 1$ , for example, represents a conversion efficiency of at least 10% [2, 29].

$ZT$  values of three or more are required for competitive energy generation [2, 30]. However, in recent years, there have been obtained  $ZT$  values of nearly three in nanostructured materials. These structures exploit its reduced dimensionality to lower the thermal conductivity of their crystal lattice ( $K_L$ ). Nevertheless, certain improvements in the materials properties, in order to increase the Figure of Merit, can be offset by undesired changes in another properties [19, 31].

Although, it is possible to observe from the equation (1) that the the maximization of  $ZT$  requires optimization of many parameters, which depend on interrelated material properties. In order to ensure a high Seebeck coefficient, is important that the semiconductor only has one type of carrier (p- or n-type) [2]. The Seebeck coefficient directly depends on the effective mass,  $m^*$ , of the charge carriers. Large effective masses produce high thermopower but low electrical conductivity. Therefore is important to balance between carriers with high effective mass and its high mobility. The power factor,  $\alpha^2 \sigma T$ , is

typically optimized in narrow-gap semiconducting materials as a function of carrier concentration (generally around  $10^{19}$  carriers/ $cm^3$ ) [6], through doping, in order to obtain the largest ZT. Figure 2.2 shows  $Bi_2Te_3$  modeled results, in which larger ZT were obtained with a carrier concentration between  $10^{19}$  and  $10^{21}$  carriers per  $cm^3$  [2, 6, 32, 33].

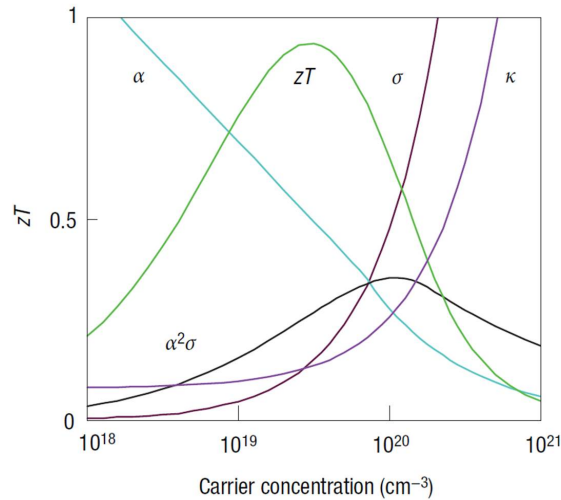


Figure 2.2: Optimization of ZT through carrier concentration tuning [2]

### 2.1.1 State-of-the-art: Materials

The selection of low cost materials with reasonable thermoelectric properties and cost-efficient preparation processes has special importance to increase the range of application of TGEs. Several materials have been shown to have great TE performance, presenting Figure of Merit above 1. However, their application is limited due to their toxicity, availability and relatively high processing and exploration costs. Moreover they often have low thermal and chemical stability [2, 8].

Bismuth Telluride ( $Bi_2Te_3$ ) has been one of the most studied TE materials. Strong covalent bonds keep the Bi and Te layers together, while the bonding of the adjacent Te layers is held by Van der Waals forces. This weaker bonding between the Te layers leads to an anisotropy on the electrical and thermal properties of this material.  $Bi_2Te_3$  presents a n-type behavior, when grown from melts which contain large amounts of tellurium, iodine or bromine. On the other hand, when growing from a melt or by zone refining, the  $Bi_2Te_3$  crystals are always non-stoichiometric and have a p-type behavior. Both p- and n-type  $Bi_2Te_3$  have a ZT of approximately 0.6 at room temperature [6, 34].

Apart from  $Bi_2Te_3$ , another widely applied TE material is the PbTe, which TE properties are isotropic. It can be doped with a wide amount of materials, for example,  $Na_2Te$

or  $K_2Te$  (acceptors), for the production of p-type materials, or and  $PbI_2$ ,  $PbBr_2$  or  $Ge_2Te_3$  (donors), in order to produce n-type semi-conductors.  $PbTe$  has ZT value of around 0.15 at room temperature, which is relatively low for a TE material. Although, for temperatures above  $420^\circ C$  (700 K), a ZT of about 0.7 can be obtained, allowing the application of this alloy in this temperature range [6, 35].

Silicon-Germanium (SiGe) alloys are materials for thermoelectric devices especially suited for application in the range of 600 to  $1000^\circ C$  [6]. Although individually Si and Ge have high thermal conductivities (150 W/m.K in the case of Si, and 63 W/m.K for Ge), SiGe alloy has a thermal conductivity of about 10 W/m.K. SiGe alloys (which best composition is  $Si_{0.7}Ge_{0.3}$ ) have large interest not only for their use on radio-isotope thermoelectric generators for space craft missions, but also for waste heat recovery applications [6, 36].

Magnesium silicide ( $Mg_2Si$ ) is another promising silicide for thermoelectric devices at temperature ranging from 100 to  $500^\circ C$  [37–39].  $Mg_2Si$  can be doped with several materials, for example, with Al, P, Sb, and Bi, resulting in ZT values up to 0.86, in the case of Bi ([40]), or even with  $Mg_2Sn$  producing a ZT of 1.1 approximately [41].

A new class of TE materials, based on metal oxides, was developed by Ohta, in 2007. It consists in a two-dimensional electron gas (2DEG) in  $SrTiO_3$ . The 2DEG demonstrates a Seebeck coefficient  $\alpha$  approximately five times higher than the bulk material and a ZT value that reaches 2.4.  $Na_2CoO_4$ ,  $CaMnO_3$ ,  $(ZnO)(In_2O_3)$ , ZnO and  $CuAlO_2$  are other new promising oxide TE materials, also developed in Japan [42, 43].

Some of the most common used TE materials, and their respective manufacturing cost and ZT values are presented in Table 2.1, which is based on the article by LeBlanc et al. [44].

Table 2.1: State-of-the-art materials used for TE applications, adapted from LeBlanc et al.[44]. Relative low temperature corresponds to  $T < 100$  °C, while relative high temperature refers to  $T > 500$  °C. ZT values were measured in a certain temperature within the respective range

Materials	Manufacturing	Cost (€/Kg)	ZT	Relative temperature
$\text{Bi}_2\text{Te}_3$	Bulk	101.30	0.74	Low
$\text{Bi}_{0.5}\text{Sb}_{1.48}\text{Te}_3$	Bulk	115.12	1.05	Low
SiGe	Bulk	625.31	0.3	High
$\text{Si}_8\text{OGe}_2\text{O}$	Nanobulk	341.67	0.53	High
$\text{Mg}_2\text{Si}_{0.6}\text{Sn}_{0.4}$	Bulk	3.72	1.05	High
$\text{Ba}_8\text{Ga}_{16}\text{Ge}_3\text{O}$	Bulk	593.08	0.36	High
$(\text{Zn}_{0.98}\text{Al}_{0.02})\text{O}$	Bulk	2.12	0.08	High
$\text{Na}_{0.7}\text{CoO}_2$	Bulk	33.15	0.52	High
$\text{Zn}_{0.25}\text{Hf}_{0.25}\text{Ti}_{0.5}\text{NiSn}_{0.994}\text{Sb}_{0.006}$	Bulk	8.94	1.38	High

The interest of TE materials for high temperature applications, have raised the demand for the research of more suitable materials. One positive feature in metals is their relatively high ratio between electrical and thermal conductivity. Concerning their limitations, oxide materials seem to be one interesting alternative, fulfilling being stable for high-temperature applications. In a general way, oxides have low mobility and high lattice thermal conductivity, due to the low atomic mass of oxygen and the strong bonding of light atoms (deriving from large differences in electronegativity), respectively. This can be seen as a disadvantage of the application of oxides as TE materials. For these reasons, is necessary to optimize the selection of materials and corresponding manufacturing processes [2, 19, 45].

The required throughput of thermoelectric material in a manufacturing process will depend on the performance of the material and the yield of the process. One of the main challenges is the high manufacturing cost of TEGs [44, 46].

### 2.1.2 State-of-the-art: Manufacturing Processes

There exist several manufacturing processes for the production of thermoelectric materials, which development has been increasing in the last years, in order to lower their processing costs. Depending on the bulk material as well as the desired properties, the thermoelectric materials can be produced either by powder processing or from a melt. However, recently, powder processing techniques have become more relevant, often using powders with micro and nanosized particles as a start material. Typically, the different

components are initially sintered and assembled to achieve the desired geometry. Then, they are applied onto the heat source, under high pressure conditions [47–49].

For powder production, the most relevant method is the ball milling of bulk materials [49]. Taking into account the processing and compaction of the thermoelectric powders, the conventional used techniques are hot pressing (HP), gas pressure sintering (GPS) and hot isostatic pressing (HIP). Most recently, spark plasma sintering (SPS) has gained more importance, not only in economic aspects but also technically. SPS has a shorter sintering time, when compared to the other conventional methods, mentioned above. However, the high heating rates of SPS, together with its high pressure and temperature conditions, often leads to the formation of internal tensions in the material. Although it is possible to reduce these internal stresses by means of an annealing process, this turns out to be an unprofitable process due to the time and energy consumed. Furthermore, there is a geometrical limitation on the TE materials produced by this technique [4, 49, 50].

Melt spinning's developed for rapid cooling of liquids such as metal melts. It is used to develop materials that require extremely high cooling rates (from  $10^1$  to  $10^7$  K/s), in order to form, metallic glasses or nanocomposites, for example. Through melt spinning, highly refined nanostructures and even amorphous phases can be obtained [51, 52].

For applications with high geometric complexity, especially at high temperatures, thermal spray has been proved to have great potential, compared with the conventional sintering processes. In particular, due to its high deposition rate and process flexibility, and also its capability of producing a shape-conformal and multi-layered structure [53, 54].

## **2.2 Zinc Oxide (ZnO)**

### **2.2.1 Basic properties and applications**

Recently, the low cost and environmental friendly ZnO ceramic has been seen as a promising TE material, due to its high thermal and chemical stability at high temperature (above  $725^\circ\text{C}$ ) [55, 56]. In materials science, zinc oxide is defined as a semiconductor in group II-VI, which covalence is between covalent and ionic semiconductors. It's large exciton binding energy (60 meV at room temperature) and wide band gap (approx. 3.37 eV at 300 K) make it a very interesting material for optical and electrical applications [57, 57–61].

The importance of ZnO in the ceramics industry has been increasing due to its hardness and piezoelectric constant, while its low toxicity, biocompatibility and biodegradability make it a material of interest for biomedicine and in pro-ecological systems [62–64]. Thanks to the piezo and pyroelectric properties of ZnO, it is applied in sensors, and as energy generator and photocatalyst in hydrogen production [65, 66]. ZnO has been proposed for a variety of applications spanning from thermoelectric, sensors, catalysis to transparent electronic materials [67]. The most common crystal structure of ZnO is the hexagonal wurtzite structure (Figure 2.3). Because of this simple structure, ZnO has a high thermal conductivity, of approx. 49 W/m.K at 300 K and 10 W/m.K at 1000 K [29], which lowers its ZT value, which can be seen as a disadvantage for TE applications [29, 55, 68].

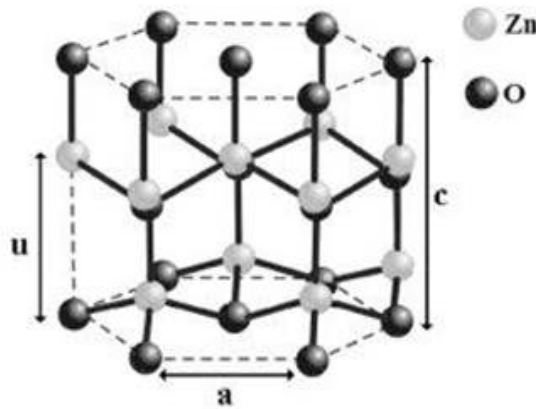


Figure 2.3: A schematic of the wurtzite ZnO crystal structure [69]

In contrast to conventional thermoelectric materials, which typically have heavy band features, n-type ZnO (e.g. Al-, Ga-doped) has a singly degenerate s-electron conduction band, with a low effective mass,  $m^* = 0,24 m_e$ , and high mobility [55]. It has been recently shown, that by doping ZnO, its thermal conductivity can be reduced, without the deterioration of its electrical conductivity [6, 55, 70, 71]. Al doping, for example, promotes the grain refinement and nanoprecipitate formation, while at the same time tuning the charge carrier concentration in order to retain a high  $\alpha^2 \sigma$  [55]. CdO doping also shows to be successful [21]. At a molar ratio of 1:9 (best composition obtained was  $\text{Zn}_{0,9}\text{Cd}_{0,1}\text{Sc}_{0,01}\text{O}$ ) resulted in a significant reduction of the thermal conductivity up to 7 times at room temperature. Compared with Al and Ga, Cd and Sc doping confer ZnO better resistance at high temperatures, without significant properties deterioration [21, 55].

Several donor dopants have been studied, which could increase electrical conductivity of ZnO-based TE materials from approximately  $5 \times 10^4$  to  $9 \times 10^4$  S/m [21, 29, 72]. However, further increase of the electrical conductivity is constrained due to the formation of

Schottky barrier (potential energy barrier for electrons formed at a metal–semiconductor junction at grain boundaries) and the limited solid solubility of trivalent cations, which in the case of Al is about 0.3 at.% [73]. Intrinsic defects such as interstitial oxygen and zinc vacancies, mostly localized in the grain boundaries, attract charge carriers which creates a depletion region. Then, an energy potential barrier is formed, which lowers the motion of the electrons [74, 75]. Therefore, to simultaneously increase the electrical conductivity and lower the lattice thermal conductivity, three possibilities emerge, based on the study of the defect design of ZnO grain structure [68, 76]:

- Decrease the amount of acceptor defects located in the grain boundaries, which lowers the Schottky barrier;
- Increase the solubility of trivalent dopants, to substitute Zn atoms in the grains, in order to increase the carrier concentration;
- Create highly defective grains, lowering the  $K_L$  by the increasing of phonon scattering.

Considering the use of dopants, the relative concentrations of the various defects depend strongly on temperature, due to the different ionization energies and diffusion coefficients. Moreover, the partial pressure of oxygen and zinc,  $p_{O_2}$  and  $p_{Zn}$ , respectively, are also very important. Hence, at high temperatures and under very reducing conditions, oxygen vacancies can predominate. On the other hand, Zinc interstitials are the predominant defects under Zn vapor rich environments. In a Zn-poor environment, at relatively low temperatures, such as 500°C, Zn evaporates easily [77]. Therefore, in order to maintain a Zn interstitial concentration, it is required to anneal in the presence of Zn vapor followed by rapid quenching [78]. Solubility of saturated Zn vapor (atoms/cm<sup>3</sup>) can be obtained by [77, 79]:

$$n = 3.4 \times 10^{20} \exp(-0.65e/kT) \quad (2)$$

Despite it can be doped both as a p-type and n-type semiconductor, the fabrication of p-type ZnO semiconductors is difficult due to the self-compensating effect from native defects (oxygen vacancies and zinc interstitial), as well as H incorporation [80, 81]. Previous studies on doping ZnO based materials and their TE properties are presented on Table 2.2.

Table 2.2: Previous studies on doping of ZnO TE materials

Reference	Type of carrier	Doping	Carrier concentration ( $\text{cm}^{-3}$ )	Power factor ( $\text{W/mK}^2$ )	Seebeck coefficient ( $\mu\text{V/K}$ )	ZT
Bian et al. (2004), [82]	p-type	N	$8.59 \times 10^{18}$	-	408.2	-
Tian et al. (2016), [68]	n-type	$\text{Al}_2\text{O}_3 + \text{MgO} + \text{TiO}_2$	$1.7 \times 10^{20}$	$8.2 \times 10^{-4}$	-93	0.9
Ohtaki et al. (1995), [83]	n-type	Al	$7.2 \times 10^{29}$	$13 \times 10^{-4}$	-180	2.4
Ohtaki (2009), [84]	n-type	Al + Ga	-	$23 \times 10^{-4}$	-250	0.65
Han (2014), [21]	n-type	$\gamma\text{-Al}_2\text{O}_3$	-	$8 \times 10^{-4}$	-140	0.17
Han (2014), [21]	n-type	CdO	$5.79 \times 10^{19}$	$6.8 \times 10^{-4}$	-150	0.3
Han (2014), [21]	n-type	$\text{Al}_2\text{O}_3 + \text{Ga}_2\text{O}_3$	-	$7.5 \times 10^{-4}$	-100	0.14

### 2.2.2 Processing

Normally oxide thermoelectric materials, as the case of ZnO based TE, are sintered by SPS. This is a rapid sintering method, which confers excellent properties compared to conventional sintering processes [85]. The SPS makes it possible to form a homogeneous microstructure because sintering at low temperature and within a short time prevents an excessive or abnormal grain growth. In addition, due to the surface cleaning effect, clean grain boundaries are obtained. Also, low temperature sintering avoid the formation of unnecessary secondary phases at the grain boundaries [86, 87].

Relatively to the ZnO coating's manufacturing processing, they have been prepared by many techniques, such as thermal evaporation, chemical vapor deposition (CVD) [88, 89], spray pyrolysis [90, 91], physical vapor deposition (PVD) [92] and sol-gel-dip-coating [93, 94]. These techniques are quite expensive or time-consuming, which is a disadvantage for industrial applications [95].

It is possible, however, via TS a production of a multilayered coating consisting in different materials, with only one technology, making it a solution of high commercial interest [95, 96]. Tului *et al.* [97] used commercial ZnO powder, with an average grain size of 0.8  $\mu\text{m}$ , agglomerated by spray drying, obtaining an average grain size of 50  $\mu\text{m}$  round sized particles, suitable for plasma spray (PS) equipment. ZnO coatings with reasonably good electrical properties were successfully produced via PS. It has been proved to be a profitable solution, capable of producing coatings with high throughput [97].

## 2.3 Thermal Spray

Thermal Spray comprises a family of coating process, which allowing the deposition a wide range of feedstock materials (such as metals and alloys, ceramics, cermets and polymers or even a combination of different materials) in a large surface area of several substrate materials at high rates. In TS, molten or partially-molten particles are accelerated towards the substrate by a gas or a mixture of gases, and projected onto a cleaned and prepared substrate. Upon impact, particles are flattened and solidified to form a structure called "splat". During the process, the splats overlap and adhere to each other producing a continuous coating [9, 98, 99].

Figure 2.4 presents an illustration of a typical thermal spray process (APS), where is shown the initial powder as feedstock material (top left) and the final coating (bottom right).

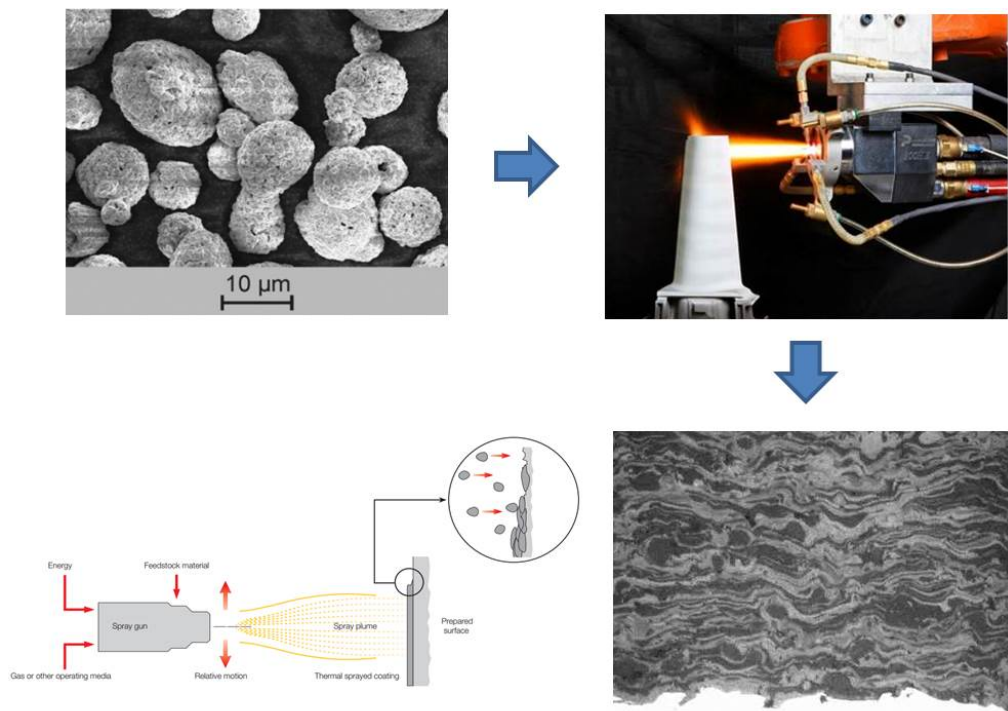


Figure 2.4: Schematic illustration of thermal spray - APS [98, 100]

In TS, the feedstock materials are heated until approximately their melting point, or even above it. They can be introduced to the process as powder, wire, rod, or even a suspension. The powder/suspension can be injected internally/externally or radially/axially (in relation to spray gun) to the flame/plasma. After the impact with the substrate, particles adhere to the surface, connecting with each other as they solidify [9, 101, 102].

The bonding mechanism of the thermal spray coatings is mainly mechanical keying or interlocking. Still, it is possible to occur local diffusion of coating material with the substrate and bonding mechanism by means of Van der Waals forces. Adequate surface preparation, in particular substrate roughness, must be taken in consideration [98, 103]. Surface area is increased and therefore coating bond strength is improved through cleaning and grit blasting. It provides a more chemically and physically active surface needed for good bonding and adhesion. The total coating thickness is controlled by generating multiple passes on the substrate [9, 103].

After deposition of the initial layer, which is directly in contact with the substrate, it is important to guarantee next coating layer bond as new droplets impact on previously solidified particles. This bonding occurs through cohesion, which is the adhesion between *splat* particles. Coating strength is influenced by porosity, oxide inclusions or unmelted particles during the deposition process. The presence of unmelted particles reduces contact area, which lower particle cohesion and decreases heat transfer. This leads

to anisotropy of coatings, a characteristic of TS coatings [9, 104, 105].

All thermal spraying processes are characterized by the combination of thermal and kinetic energy, which are essential for coating deposition. Depending on the thermal energy source, TS processes are categorized to: compressed gas expansion (Cold spray), combustion - flame spray, high velocity oxy fuel (HVOF), high velocity air-fuel (HVOF) and detonation gun, and electrical discharge - arc spray and APS. Kinetic energy is produced by the constriction of the hot gas stream through a nozzle [9, 106]. A schematic of the relation between process temperature and velocity for the different TS processes is shown in Figure 2.5.

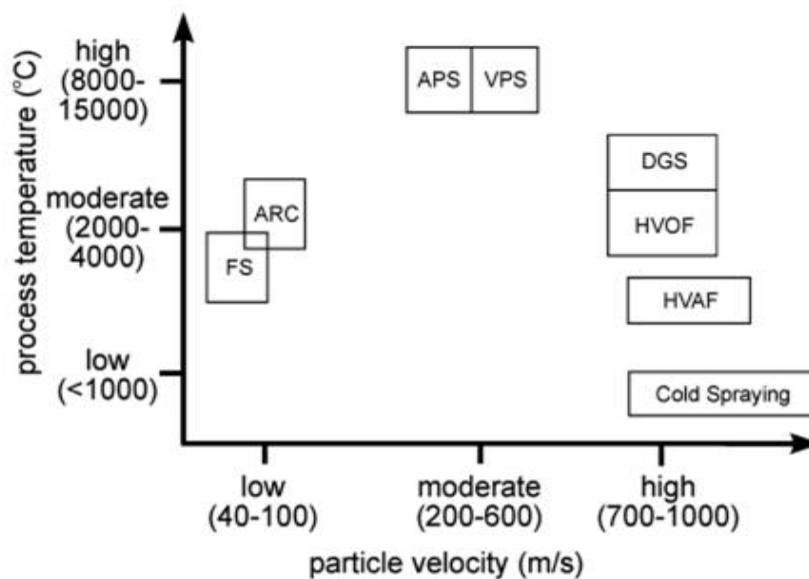


Figure 2.5: Schematization of relationship between thermal and kinetic energy for the different TS processes (FS – Flame spraying, ARC – Arc spraying, APS/VPS – atmospheric/vacuum plasma spraying, DGS – detonation gun spraying, HVOF/HVOF – high velocity oxy-fuel / air-fuel spraying [104])

The high temperature of PS is particularly suitable for materials with a high melting point and high thermal stability, such as ceramics [101, 107].

### 2.3.1 Atmospheric plasma spray

APS was patented by Giannini and Ducati in 1960, as well as by Gage in 1962, which torch was based on Gerdien-type plasma generator (Gerdien and Lotz, 1922). It is characterized for being the most flexible of all thermal spray processes, due to the high variety of materials that can be coated with this method. The plasma is normally generated by the ionization of an inert gas (such as argon, or a mixture of argon and hydrogen) through

an arc, produced by continuous current (DC). This results in temperatures from 6000°C to 15000°C, in the powder heating zone [4, 98, 102, 108].

In this process, the feedstock material is externally supplied and the primary plasma forming gas is used as a carrier to transport the powder up to the plasma stream, as it is possible to see in the Figure 2.6, where a typical PS gun is shown.

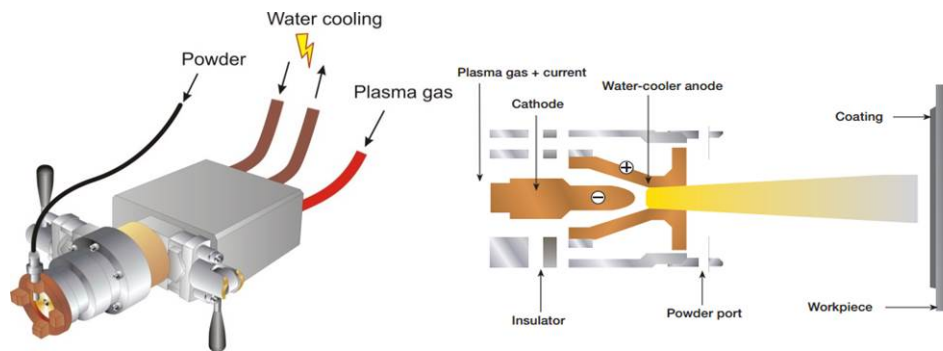


Figure 2.6: Schematization of a plasma equipment [4, 108]

### 2.3.1.1 Process variables

Manipulation of variables such as standoff distance, gas mixing, powder feeding rate and applied current should be taken in consideration to achieve the best coating morphology:

- *Standoff distance*

The adjustment of the standoff distance is important to ensure enough adhesion strength of the coating to the substrate. The increase of the spraying distance will lead to a higher cooling rate and deceleration of the particles, which will result in a lack of adhesion to the substrate. However, if the spraying distance is too short, the connection between coating and substrate will overheat, and generate internal stresses within the coating, lowering the adhesion strength [109]. In general, the increase of the standoff distance will promote an increase of the coating's hardness, due to the sufficient time for the particles to dwell and melt, producing denser coatings. At short distances, substrate overheating can cause the excessive splashing of molten particles, and therefore, less dense coatings, with lower hardness values. On the other hand, longer spray distances lead to a decrease in the velocity of impact and, consequently, to a higher coating porosity [102, 109, 110]. It is generally accepted by various experimental results that there exists a critical velocity, which the particle velocity has to exceed in order to successfully obtain a coating, as shown in Figure 2.7 [111, 112]

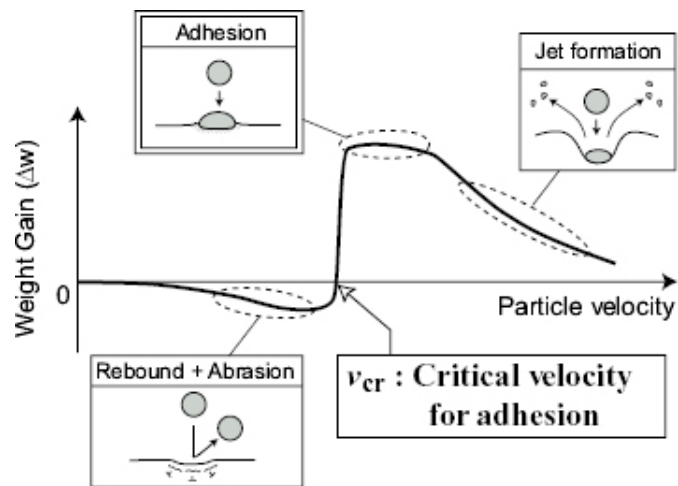


Figure 2.7: Concepts of critical velocity [112]

Jadidi *et al.* [113] tracked the suspended particles to study the effect of substrate shape and curvature on in-flight particle velocity, temperature, and trajectory in suspension PS. The obtained results are presented in Figure 2.8.

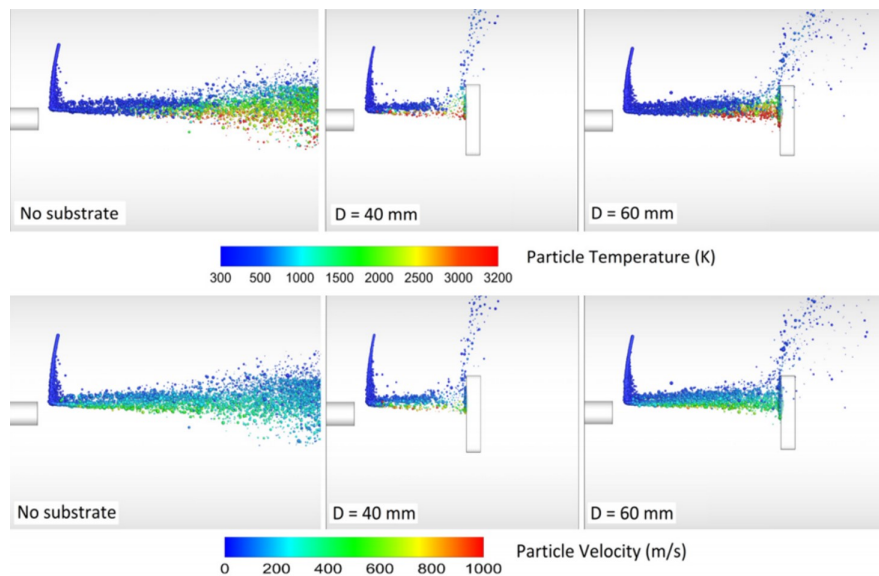


Figure 2.8: The droplet/particle temperature and trajectory in suspension plasma spray at different standoff distances ( $D$ ) [114]

It can be observed that particles' highest temperature is only achieved at a certain distance (60 mm on this case). The same happens with the particle's velocity.

- *Powder feeding rate*

The increase of the powder feeding rate often results in higher deposition rates, increasing the coating's adhesion strength and hardness. Although, is important to

have other conditions in account, in order to obtain homogeneous and low porosity coatings. For example, if the feeding rate is too high and there is not enough current to melt the sprayed feedstock material, there will be unmelted particles which lead to an increase of film porosity and a decrease in coating adhesion [98, 110].

- *Current*

By increasing the current value, the temperature of the process will also be increased. Therefore, more particles will be melted, resulting in higher adhesion strength and hardness of the deposited coatings. Furthermore, if the current is too high, there may be an excessive heating of the substrate, which in turn could affect substrate properties [98, 102, 109].

- *Gas composition*

Depending on the used coating material and the desired properties, several types of gases can be selected to form the plasma. A comparison between the properties of the most common plasma gases is presented on Table 2.3.

Table 2.3: Plasma gas comparison [115]

	N <sub>2</sub>	Ar	He	H <sub>2</sub>
<i>Flame temperature (K)</i>	10,000	20,000	25,000	13,000
<i>Heat conductivity (mK/m.K)</i>	26	18	155	183
<i>Ionization energy (KJ/mol)</i>	1402	1520	2372	1312

Generally, a mixture of nitrogen with 5% to 10% of hydrogen is used, providing the maximum heat transfer to the particles. It also promotes a reduction of the process cost. Although, for certain materials, the use of nitrogen may result in an undesirable reaction. In this case, argon is a reasonable alternative [98]. Argon/helium (20 to 50 vol% of He) mixtures are often used. Helium increases the thermal conductivity of the plasma stream, increasing heat capability of the plasma, even though it has a relative high cost. Argon/hydrogen (5 to 15% H<sub>2</sub>) plasmas have higher enthalpy than argon/helium plasmas due to the diatomic structure of hydrogen and its reduced mass, which results in high collisional cross section [98, 102, 109].

Common plasma gases compositions in ascending order of enthalpy are presented below [109]:

- Argon (Ar);

- Argon/Helium (Ar/He);
- Argon/hydrogen (Ar/H<sub>2</sub>);
- Nitrogen (N<sub>2</sub>);
- Nitrogen/hydrogen (N<sub>2</sub>/H<sub>2</sub>);

### 2.3.1.2 Feedstock material

Conventional APS process uses powders as a feeding material, which size range between 25 and 45  $\mu\text{m}$ . The dimension of these particles often lead to certain limitations in the achievable microstructural features, since nano-scaled powders cannot be directly used in this process due to their low flowability. The substitution of the conventional spray powders by suspensions allows the direct use of finely dispersed powders and the production of nanostructured coatings [116, 117].

The advantages of using suspensions, when compared with powders as a feeding material include [118]:

- Coatings with improved properties;
- Potential to fill the technological gap between thin films and TS coatings, allowing the possibility to deposit coatings which thickness range between 5 to 50  $\mu\text{m}$ ;
- Lower surface roughness;
- Lower coating anisotropy;
- Coatings with higher density;

In relation to hardware, a suspension feeder and a suitable suspension injector (Figure 2.9) are required for spraying with suspensions.



Figure 2.9: APS and HVOF suspension thermal spray injectors, with inner diameters of 0.2 and 0.3 mm [119]

Figure 2.10 shows a “stand alone” suspension feeder spraying system developed by Fraunhofer IWS, which can be easily integrated into a conventional TS equipment. Material containers are pressurized, which allows a precise, constant and pulse-free material feeding [119, 120].



Figure 2.10: Three-vessels suspension feeder (Fraunhofer IWS) [119]

The suspension feeder is composed of three vessels, where two of them contain the desired suspensions, while the third contains a cleaning liquid (mostly water). Integrated agitators ensure stable storage of the suspensions and prevent sedimentation in the containers (Figure 2.11). This feeding system is suitable for industrial applications, since the three-vessels configuration allow an “interruption-free” process, if the same suspension is use in both vessels. On the other hand, if two different suspensions are used, a multi-layered coating can be produced. It is also possible to use simultaneously two different suspensions [121].

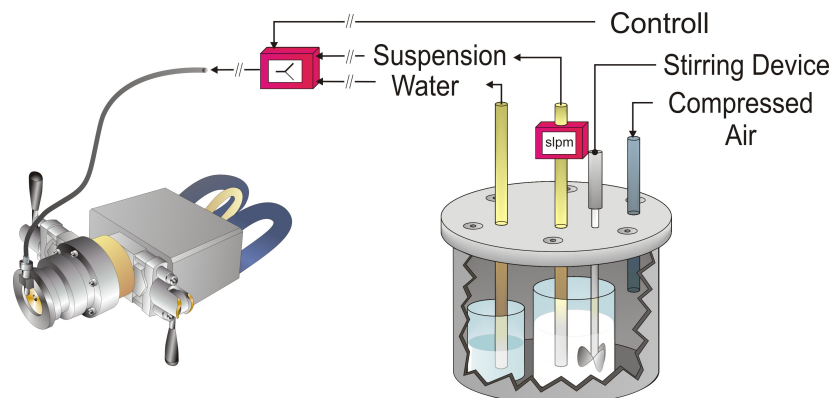


Figure 2.11: Schematization of a suspension feeding system with integrated agitator three-vessels

Suspension atmospheric plasma spraying (S-APS) is a new promising processing method which employs suspensions of sub-micrometer particles as feedstock. The associated solvent, present in the suspension, is vaporized before the powder particles reach the substrate. As a result, this process requires more enthalpy per gram of deposited material, compared with conventional APS. Thus, ethanol can be injected, working as an additional enthalpy source as its combustion heat is considerably above its evaporation enthalpy. The resulting temperature increase depends on the depth of injection into the plasma jet. Regarding plasma velocity, the injection of ethanol led to a gain of momentum and therefore to higher speeds. Additionally, due to the reduced particle size of the suspensions, the particles are more sensitive to temperature gradients. Therefore, in order to prevent their solidification before reaching the substrate, in S-APS, standoff distances are generally shorter [117, 122, 123].

Instead of ethanol, water based suspensions are also available for TS processes. Their absence of organic solvents provides an easier and safer handling of the suspensions, and water based suspensions lower cost, compared to the use of ethanol, is also advantageous for TS in industrial scale [124].

Concerning the use of suspensions in thermal spray processes, it is required to respect some suspension parameters in order to obtain a high quality coating and to ensure the stability of the process. The main goal is to create a colloidal-chemical stable suspension with the following characteristics [125]:

- High flowability and low viscosity, below 10 MPa.s, so that the suspension can be fed at constant feed rate, and process stability is guaranteed;
- High stability, i.e. sedimentation rate of particles below 1 mm/h;
- Zeta potential higher than 30 mV (absolute value) in order to avoid particle agglomeration;
- The pH value between 4 and 10 to prevent the corrosion of hardware components.

# Chapter 3

## Experimental Procedure

The practical component of this dissertation focused on the production of dense ZnO coatings via TS. This experimental procedure consisted in a study of the TS processes in order to reproduce the conditions in an industrial environment. Initially, the both powder and substrate materials were characterized in order to plan a coating strategy.

To simplify, during this study, the coatings produced by powder deposition were described as APS, and the coatings produced by suspension deposition were designate as S-APS.

### 3.1 Materials

#### 3.1.1 Powder

The powder available for this study was a commercially available ZnO doped with Al (2%) provided by the company Hereaus, normally used for the production of sputtering targets. Since no more information about the powder was available, initially it was characterized. Particle size distribution, was evaluated via laser diffraction, using a MasterSizer 2000 for 3 minutes. Powder particles were characterized using a scanning electron microscope (SEM) and its chemical composition was also analyzed by energy dispersive X-ray spectroscopy (EDS).

#### 3.1.2 Suspension

The previously used ZnO powders with the same composition were used by Fraunhofer IKTS in order to produce the deposited suspension. After grinding, the particles were sieved, until obtain particles below 20  $\mu\text{m}$  of diameter.

### 3.1.3 Substrate

All experiments were conducted using  $30\text{mm} \times 20\text{mm}$  flat low carbon steel as substrates, which were sand blasted using Corundum EFK40 particles and degreased with ethanol ( $\text{C}_2\text{H}_6\text{O}$ ) before deposition. However, the used substrate material was not aim of study, since, as mentioned on the literature ([3, 9]), TS allows the coating of wide range of substrate materials.

## 3.2 Coating process

Due to the powder granulometry, characterized by a  $d_{10}$  and a  $d_{90}$  of  $24\ \mu\text{m}$  and  $78\ \mu\text{m}$ , respectively, as well as the high melting point of ZnO, APS was the the first approach as a TS process. Several spray parameters were tested using a F6 single-cathode torch from GTV GmbH (Luckenbach, Germany). For the first experiment, the production route for ZnO powder deposition was based on a previously studied sprayed coatings in the  $\text{TiO}_2$  system [126]. Since the melting point of ZnO is  $1975^\circ\text{C}$  [127], which is similar to  $\text{TiO}_2$  ( $1843\ ^\circ\text{C}$  [128]), this seemed to be an appropriate starting point. Based on the used parameters, ZnO deposition was parameterized by means of a DoE.

### 3.2.1 Design of Experiments - APS

For the DoE, the influence of different process variables on the coating properties will be quantified and the process optimized accordingly.

To simplify the procedure and to study the influence of the main variables that have influence on APS process, other parameters were fixed (Table 3.1). After the first deposition, an additional experiment was performed, with higher powder feeding rate and more torch passes to have at least 100 in thickness for better characterization <sup>1</sup>.

---

<sup>1</sup>In order to optimize the parameters for the next experiment, four samples were tested with a feeding rate of 30 g/min and 30 torch passes

Table 3.1: Fixed spray parameters for APS DoE

<i>Relative torch speed (m/min)</i>	100
<i>Trace offset (mm)</i>	5
<i>Powder injector diameter (mm)</i>	1.8
<i>Powder feeding rate (g/min)</i>	25 (30 <sup>1</sup> )
<i>Torch passes</i>	10 (30 <sup>1</sup> )
<i>Angle of deposition</i>	90°
<i>Cooling</i>	3 stationary Air Jets and 2 in plasma torch

In terms of the variable parameters, first, the factors and interaction between factors, which have influence on the coating properties, were identified. Therefore, to understand how K factors affect a process and how these factors interact with each other, the optimal approach is the  $2^k$  full factorial analysis [129]. The gas composition, such as argon and hydrogen content, arc current (A) and spray distance (mm) were the chosen variables in this DoE, since they have a great influence on the particle state (velocity and temperature). This would mean a  $2^4=16$  experiments. First, a low (-) and a high (+) level for each parameter were defined. Then, alternating the levels of the factors, the experimental matrix presented in Table 3.2 was obtained. Through this strategy, all combinations were tested.

Table 3.2: Matrix of experiments of APS coatings

	<i>Arc Current (AC)</i>	<i>Spray Distance (SD)</i>	<i>Ar (%)</i>	<i>H<sub>2</sub> (%)</i>	<i>Result</i>
1	-	-	-	-	Y <sub>1</sub>
2	+	-	-	-	Y <sub>2</sub>
3	-	+	-	-	Y <sub>3</sub>
4	+	+	-	-	Y <sub>4</sub>
5	-	-	+	-	Y <sub>5</sub>
6	+	-	+	-	Y <sub>6</sub>
7	-	+	+	-	Y <sub>7</sub>
8	+	+	+	-	Y <sub>8</sub>
9	-	-	-	+	Y <sub>9</sub>
10	+	-	-	+	Y <sub>10</sub>
11	-	+	-	+	Y <sub>11</sub>
12	+	+	-	+	Y <sub>12</sub>
13	-	-	+	+	Y <sub>13</sub>
14	+	-	+	+	Y <sub>14</sub>
15	-	+	+	+	Y <sub>15</sub>
16	+	+	+	+	Y <sub>16</sub>

Additionally, in order to study the linearity of the influence of the variable parameters on the results, a center point was defined. Table 3.3 displays the low (-) and high (+) level of the chosen variable parameters (mentioned above) for ZnO powder deposition.

*Table 3.3: Variable parameters for APS DoE*

<b>Parameter</b>	<b>Low level (-)</b>	<b>High level (+)</b>
<i>Current (A)</i>	400	530
<i>Spray distance (mm)</i>	110	120
<i>Argon content (%)</i>	40	46
<i>Hydrogen content (%)</i>	4	6

After this values being processed, plots of interaction between the responses of the parameters were achieved with the software *Minitab*. An interaction plots based on a matrix of interactions (Table 3.4) shows the impact that changing the settings of one factor has on another factor [130]. This interaction can increase or lower main effects, and therefore it should be evaluated. With statistical algorithms, it is possible to achieve interactions between the four parameters in the chosen response, which is coating thickness.

Table 3.4: Matrix of interactions

	<i>AC</i>	<i>SD</i>	<i>Ar</i>	<i>H<sub>2</sub></i>	<i>AC vs SD</i>	<i>AC vs Ar</i>	<i>SD vs Ar</i>	<i>AC vs SD vs Ar</i>	<i>AC vs H<sub>2</sub></i>	<i>SD vs H<sub>2</sub></i>	<i>AC vs SD vs H<sub>2</sub></i>	<i>AC vs SD vs Ar vs H<sub>2</sub></i>
1	-	-	-	-	+	+	+	-	+	+	-	+
2	+	-	-	-	-	-	+	+	-	+	+	-
3	-	+	-	-	-	+	-	+	+	-	+	-
4	+	+	-	-	+	-	-	-	-	-	-	+
5	-	-	+	-	+	-	-	+	+	+	-	+
6	+	-	+	-	-	+	-	-	-	+	+	+
7	-	+	+	-	-	-	+	-	+	-	+	+
8	+	+	+	-	+	+	+	+	-	-	-	-
9	-	-	-	+	+	+	+	-	-	-	+	-
10	+	-	-	+	-	-	+	+	+	-	-	+
11	-	+	-	+	-	+	-	+	-	+	-	+
12	+	+	-	+	+	-	-	-	+	+	+	-
13	-	-	+	+	+	-	-	+	-	-	+	+
14	+	-	+	+	-	+	-	-	+	-	-	-
15	-	+	+	+	-	-	+	-	-	+	-	-
16	+	+	+	+	+	+	+	+	+	+	+	+

### 3.2.2 Design of experiments - S-APS

After optimization of the APS process, a suspension with the same composition will be used as feedstock material in order to obtain coatings with higher density.

Additionally, in order to obtain denser coatings, another experiment was conducted using S-APS as an alternative ZnO deposition strategy. For this experiment, the previous deposited ZnO powder was grinded to reduce the size of its particles and dispersed in an aqueous suspension (water).

As mentioned in the bibliography [122, 123], for the use of suspensions, due to reduced size of their particles, the used spraying distances were lower than in the previous experiment, described in 3.2.1. In relation to the feed rate of the suspension, this variable was kept fixed in 40 ml/min. Relatively to the other variables, the best results of the previous experiment (ZnO powders) were used for further comparison between powder and suspension deposition. The fixed parameters for ZnO suspension spraying by S-APS are presented in Table 3.5.

*Table 3.5: Fixed spray parameters for S-APS DoE*

<i>Relative torch speed (m/min)</i>	100
<i>Trace offset (mm)</i>	3
<i>Suspension injector diameter (mm)</i>	0.25
<i>Suspension feeding rate (ml/min)</i>	45
<i>Torch passes</i>	30
<i>Angle of deposition</i>	90°
<i>Cooling</i>	3 stationary Air Jets and 2 in plasma torch
<i>Hydrogen content (%)</i>	13

For better deposition results, in this experiment the hydrogen content was kept high (13%), in order to increase the thermal energy transmitted to the sprayed particles, varying only the content of argon.

In S-APS experiment, regarding the gas composition, only argon content was variable, while hydrogen was kept fixed. Additionally to Ar content, arc current (A) and spray distance (mm) were the chosen variables in this DoE for S-APS, due to their high influence on the particle state (velocity and temperature). This would mean a  $2^3=8$  experiments. First, a low and a high level for each parameter were defined. Then, alternating the levels of the factors, the experimental matrix presented on Table 3.6 was obtained.

Table 3.6: Matrix of experiments of S-APS

	<i>Arc Current (AC)</i>	<i>Spray Distance (SD)</i>	<i>Ar (%)</i>	<i>Result</i>
1	-	-	-	Y <sub>1</sub>
2	+	-	-	Y <sub>2</sub>
3	-	+	-	Y <sub>3</sub>
4	+	+	-	Y <sub>4</sub>
5	-	-	+	Y <sub>5</sub>
6	+	-	+	Y <sub>6</sub>
7	-	+	+	Y <sub>7</sub>
8	+	+	+	Y <sub>8</sub>

A center point was also defined, in order to study the linearity of the influence of the variable parameters on the results.

Table 3.7 summarizes the DoE of the variable spray parameters with their respective low and high levels.

Table 3.7: Variable parameters for S-APS DoE

<b>Variable</b>	<b>Low level (-)</b>	<b>High level (+)</b>
<i>Current (A)</i>	530	600
<i>Spray distance (mm)</i>	30	50
<i>Argon content (%)</i>	35	40

The results from the 8 experiments can be combined, in order to determine the influence of the three principal effects and the influence of the interaction between the different factors (Table 3.8).

Table 3.8: Matrix of interactions of S-APS

	AC	SD	Ar	AC vs SD	AC vs Ar	SD vs Ar	AC vs SD vs Ar
1	-	-	-	+	+	+	-
2	+	-	-	-	-	+	+
3	-	+	-	-	+	-	+
4	+	+	-	+	-	-	-
5	-	-	+	+	-	-	+
6	+	-	+	-	+	-	-
7	-	+	+	-	-	+	-
8	+	+	+	+	+	+	+

### 3.3 Coating characterization

After a visual inspection, all samples were initially characterized according to their thickness.

#### 3.3.1 Thickness measurement

The thickness measurement was performed by means of Eddy current (conductivity measurement), using a Fischer Dualscope (Figure 3.1). This equipment was first calibrated according to equipment specifications.

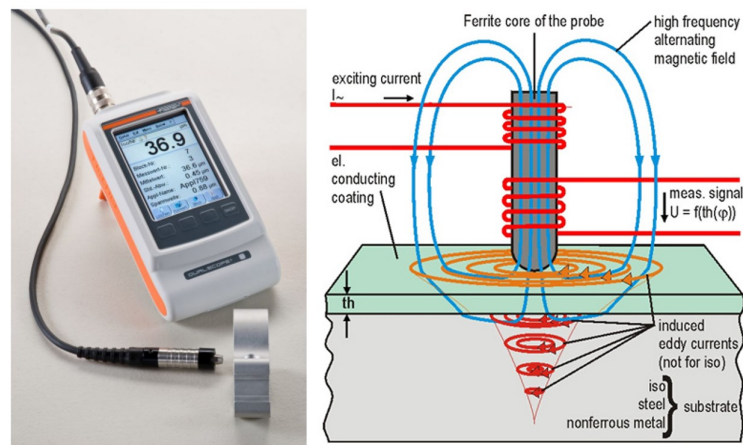


Figure 3.1: Fischer Dualscope equipment (left) and respective working principle (right) [131]

According to the thickness results, best APS and S-APS samples were chosen for further analysis.

### 3.3.2 Metallographic preparation for optical and electron microscopy analysis

After deposition, the best samples were properly prepared for optical microscopy (OM) and SEM analysis. The adopted metallographic preparation consists in the following steps:

- In order to avoid coating damage during the cut operation, the samples were initially “cold mounted” using a two-part epoxy resin. Mounting a specimen provides a safe, standardized, and ergonomic way by which to hold a sample during the following grinding and polishing operations. The hardening stage lasted approximately 24 hours.
- After hardening, the samples were cut into the zone to be analyzed. On this step, a high precision saw was used in automatic mode, allowing a slow cutting speed (0,030 m/s).
- The cut specimen is successively grinded with finer and finer abrasive silicon carbide paper at 300 rpm, using water as a lubricant. The sequence of SiC abrasive papers, following the European Grit number (P-Grade) [132] was: P320, P800, P1000 and P4000. Each specimen was rotated 90 degrees and continually ground until all the scratches from the previous grinding direction were removed.
- The next step was the rough polishing, which purpose is to remove the damage produced during cutting and grinding. Therefore, using a diamond suspension with a grain size of approximately 1  $\mu\text{m}$  in a polishing cloth, the samples were polished at 150 rpm.
- The final stage consisted in polishing manually using a Colloidal silica suspension with particles of approximately 0,06  $\mu\text{m}$  size in a OP-Chem<sup>®</sup> of neoprene, allowing further SEM analysis.

### 3.3.3 OM and SEM analysis

For the study of the coatings morphology, the cross section of the APS coatings were examined by OM, using a Keyence digital microscope VHX-6000. In the case of S-APS, the cross section was SEM analysis was performed at Centro de Materiais da Universidade do Porto (CEMUP) using a FEI Quanta 400FEG ESEM with a coupled EDS. For the study of the surface morphology all samples were analysed by SEM at the Fraunhofer Institute, using a Jeol JSM-6400 SEM configured with a Company Thermo EDS system.

### 3.3.4 Chemical composition

Coating's chemical composition was studied through the EDS equipment, as mentioned above. Additionally, an X-ray powder diffraction (XRD) was made, using as equipment a D8 Advance by Bruker AXS GmbH. XRD patterns were recorded using a Cu K $\alpha$  radiation source with a wavelength of 1.54060 nm. The analysis of the resulting spectra, using both *Origin* and *Match!* softwares, allowed to observe the influence of the APS process in the deposited coating. In addition, the interaction between the particles sprayed with the plasma and the surrounding atmosphere was studied.

### 3.3.5 Mechanical properties

Hardness tests were accessed with a Vickers indenter, using a load of 0.025 kgf (HV 0.025), during 15 seconds at room temperature, according to the standard NP EN ISO 6507-1:2011, using a Struers Duramin durometer. All indentations were made in the cross section of the samples.

However, in thermal spray coatings, a low-load microhardness indicates the degree of individual lamellae melting and can be influenced by small pores, while high-load measurements describe the overall coating in which the hardness depends on the interlamellar contact strength and also the porosity [98]. Therefore, in order to obtain better results regarding the influence of the porosity on the overall coating, a HV 0.3 (3 N) measurement was conducted in the thickest samples of APS and S-APS coatings.

# Chapter 4

## Results and Discussion

### 4.1 Material characterization

#### 4.1.1 Powder

For the first experiment, it was deposited ZnO commercially available powder doped with  $\text{Al}_2\text{O}_3$ . Powder's respective particle size distribution, evaluated via laser diffraction, is shown Figure 4.1.

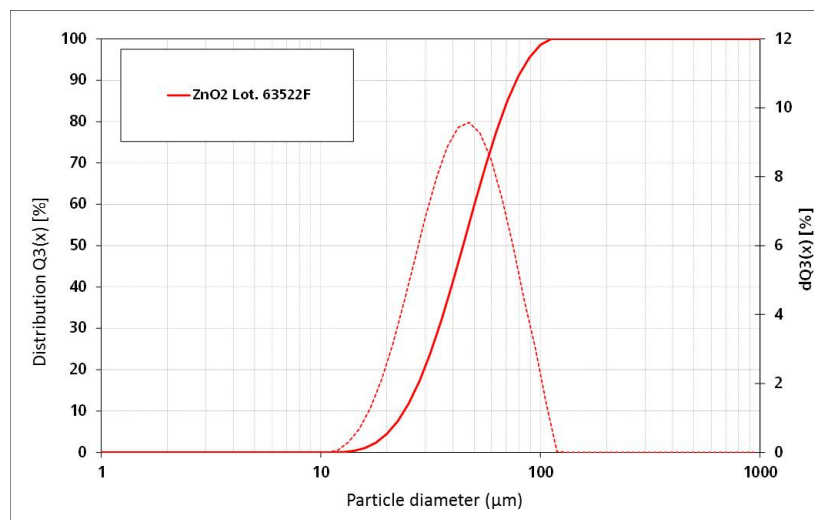


Figure 4.1: ZnO particle size distribution

Through analysis of Figure 4.1, it is possible to observe that the particle size follows a Gaussian distribution, where values 80% of the particles are between 24 μm and 78 μm, with a mean size of 44 μm ( $d_{10} = 24 \mu\text{m}$ ,  $d_{50} = 44 \mu\text{m}$ ,  $d_{90} = 78 \mu\text{m}$ ).

Figure 4.2 shows the typical powder morphology for an agglomerated and sintered (a&s) particles, which was characterized using by SEM and EDS. Besides the round

shaped morphology, the particle size distribution coincides with the laser diffraction results.

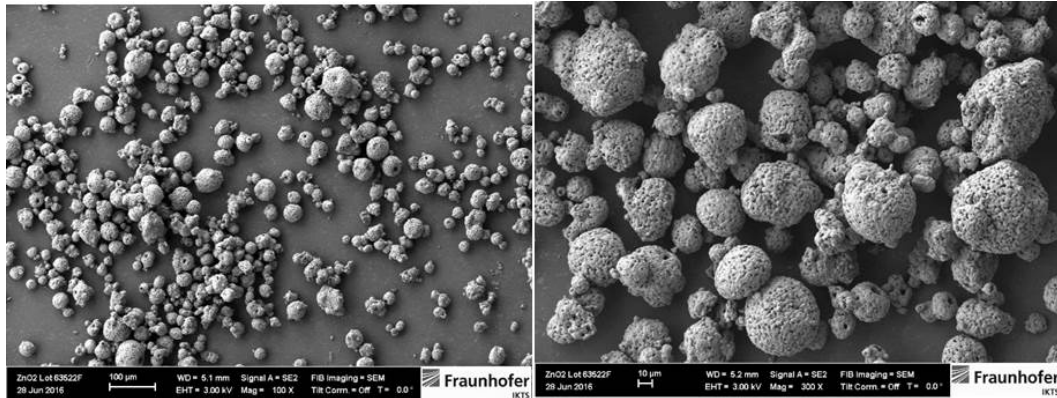


Figure 4.2: SEM images of the surface of ZnO powder

The qualitative EDS analysis (Figure 4.3) suggests that ZnO powder was doped with  $\text{Al}_2\text{O}_3$ .

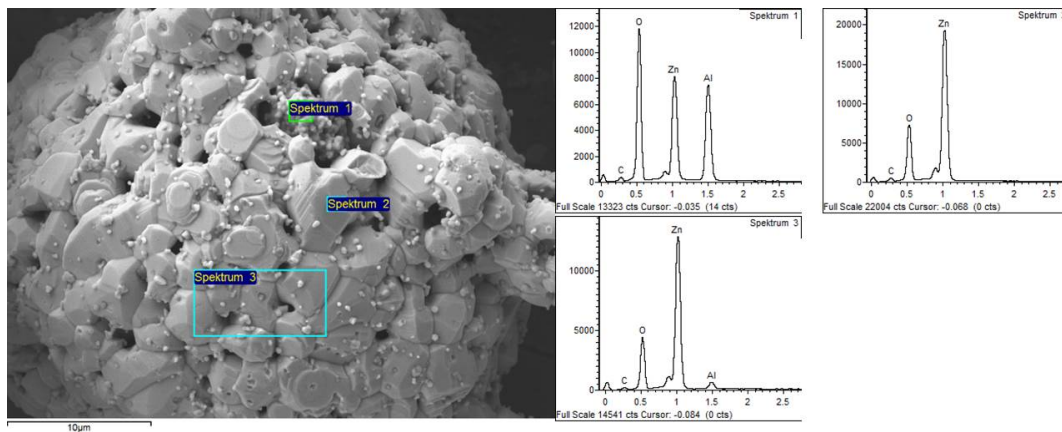


Figure 4.3: SEM images of ZnO powder and respective EDS analysis

## 4.1.2 Suspension

Regarding the use of suspensions, one of the main parameters to take into account is its viscosity, which was measured by a vibro viscometer (SV-10). Viscosity should be lower than 10 mPa.s, so that the suspension can be fed at constant feed rate, and process stability is guaranteed [125]. The used suspension has a viscosity of 4.92 mPa.s, ideal for thermal spray processing. Other main characteristics of the produced suspension are presented on Table 4.1.

Table 4.1: ZnO suspension characteristics

Mass (g)	4147
Solids content (%)	49.35
pH	9.53
Viscosity (mPa.s)	4.92 (at a shear rate of 240 /s)

Regarding the particle size distribution, these results are presented in Figure 4.4.

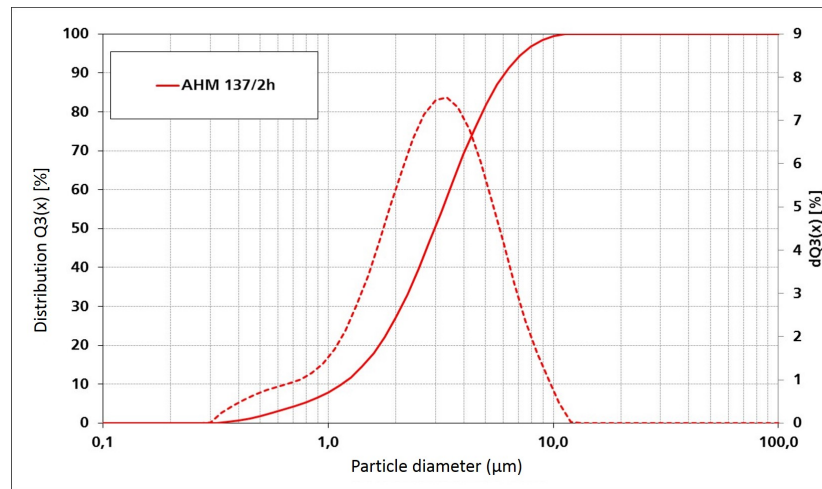


Figure 4.4: ZnO suspension particle size distribution

Figure 4.4 exhibits a particle size distribution which follows a Gaussian distribution, where values 80% of the particles are between 1.149  $\mu\text{m}$  and 6.098  $\mu\text{m}$ , with a mean size of 2.973  $\mu\text{m}$  (( $d_{10} = 1.149 \mu\text{m}$ ,  $d_{50} = 2.973 \mu\text{m}$ ,  $d_{90} = 6.098 \mu\text{m}$ )).

## 4.2 APS coatings Characterization

### 4.2.1 Thickness measurement

According to the DoE, the results from the APS experiment with the different combinations of deposition parameters are shown in Table 4.2.

Table 4.2: Thickness and deposition per pass results from APS deposition

Sample	Current (A)	Ar (%)	H <sub>2</sub> (%)	SD (mm)	Thickness (μm)	Standard deviation
APS1	400	40	4	110	11	2
APS2	530	40	4	110	21	3
APS3	400	40	4	120	8	0.7
APS4	530	40	4	120	20	3
APS5	400	46	4	110	2	0.8
APS6	530	46	4	110	8	1
APS7	400	46	4	120	1	0.4
APS8	530	46	4	120	9	0.9
APS9	400	40	6	110	12	3
APS10	530	40	6	110	32	3
APS11	400	40	6	120	9	2
APS12	530	40	6	120	30	3
APS13	400	46	6	110	6	1
APS14	530	46	6	110	23	2
APS15	400	46	6	120	3	0.5
APS16	530	46	6	120	21	2

In this experiment, APS10 sample have the thicker coating, followed by APS12. By the analysis of Table 4.2 and Figure 4.5, is possible to observe, in a general way, that the increase of the spray distance (SD) lowers the deposition rate. This was expected, since there may be a greater loss of thermal and kinetic energy of the particles for longer distances. Regarding the gas composition, better results were achieved for an Ar:H<sub>2</sub> ratio of 40:6. H<sub>2</sub> has higher thermal conductivity [115] than Ar, which allows a better homogeneity of the plasma heat among the particles. From the present results, the influence of the variable parameters on the coating thickness was studied (Figure 4.5), using Minitab software. It is then observed that larger content of H<sub>2</sub> and higher currents promote thicker coatings, due to the higher energy input.

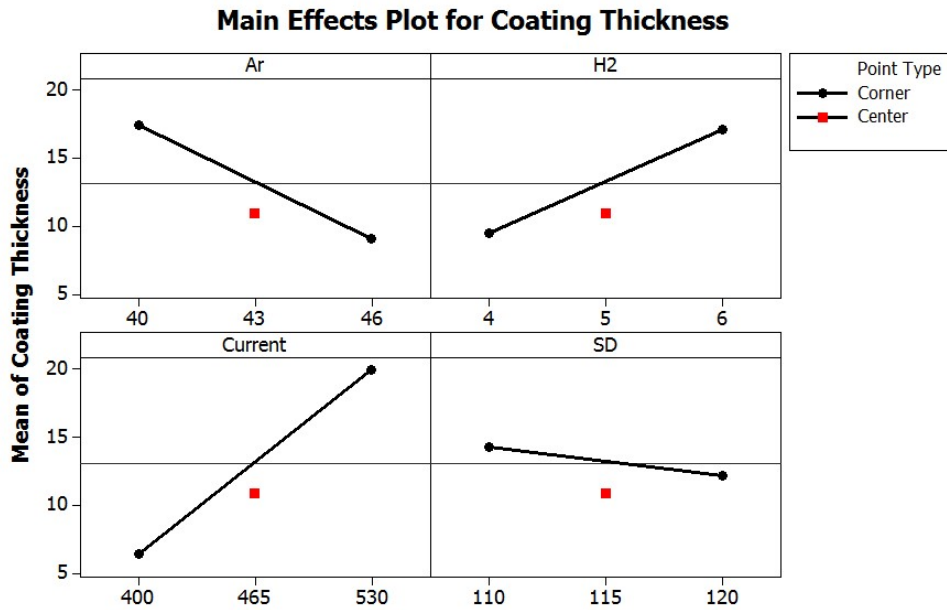


Figure 4.5: Influence of variable spray parameters in coating thickness

By Figure 4.5 analysis, is possible to observe that the variable with the greatest positive influence on the thickness of the coating is the current, followed by the H<sub>2</sub> content. As for the mount of Ar and spray distance, both variables have a negative effect on the thickness of the coating, mainly Ar content.

According to the DoE, the achieved plots of interaction between the parameters are presented in Figure 4.6.

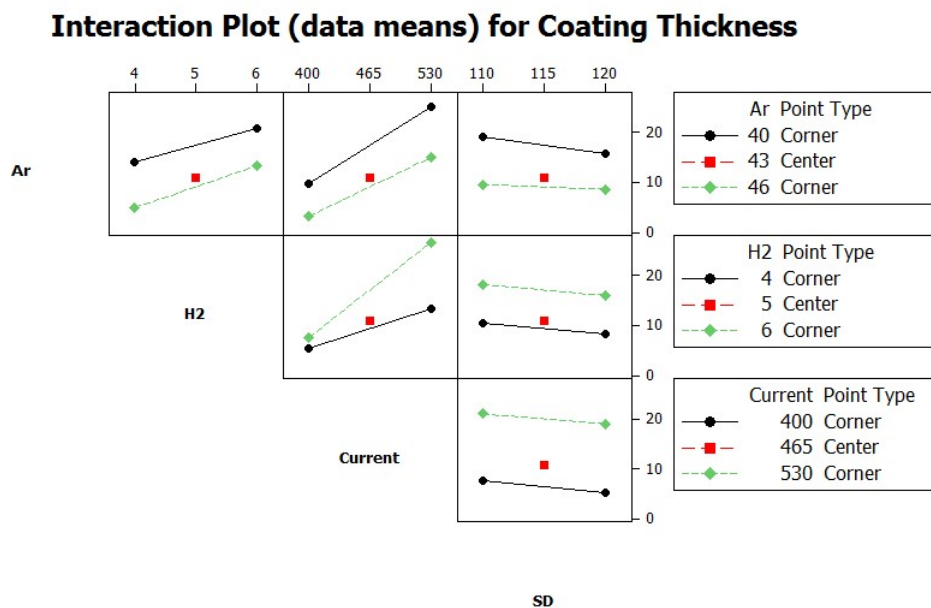


Figure 4.6: Interaction between APS variable spray parameters in coating thickness

In this interaction plot, it is visible that green and black lines are almost parallel. This indicates that all variables are independent from each other, having no significant interaction effect of the interaction between them. However, the slope of the line for the greatest H<sub>2</sub> content (green line) is slightly steeper. Therefore, it could be concluded that the current has a greater effect when the highest H<sub>2</sub> content is used (6 %).

Therefore a strategic optimization would be the increase of used current and H<sub>2</sub> content, as well as the decrease of the Ar content and of the spray distance. For that reason, other experiments were conducted in order to optimize the thickness values.

First, for the best condition of the previous experiment (samples APS10 and APS12), the value of the spray rate was also increased from 25 to 30 g/min, and the spray distance was decreased, resulting APS19 and APS20 samples. Additionally, since it was observed that compositions gas compositions richer in hydrogen and higher current values result in thicker coatings, two other samples (APS21 and APS22) were sprayed with a Ar:H<sub>2</sub> ratio of 35:13 and a current of 600 A. On this experiment, all samples were sprayed with 30 passes (instead of the previous 10), to increase the deposition ratio, which results are presented on table 4.3.

Table 4.3: Variable parameters for additional APS experience

Sample	Current (A)	Ar (%)	H <sub>2</sub> (%)	FR (g/min)	SD (mm)	Thickness (μm)	Standard deviation
APS19	530	40	6	30	90	152	5
APS20	530	40	6	30	110	124	4
APS21	600	35	13	25	100	137	5
APS22	600	35	13	25	110	140	4

Samples APS10 with APS20 were sprayed with the same conditions, but with different number of passes as well as different powder feeding rate. The increase of these two variables resulted in a thicker, homogeneous and denser coating as is possible to observe in Figure 4.7.

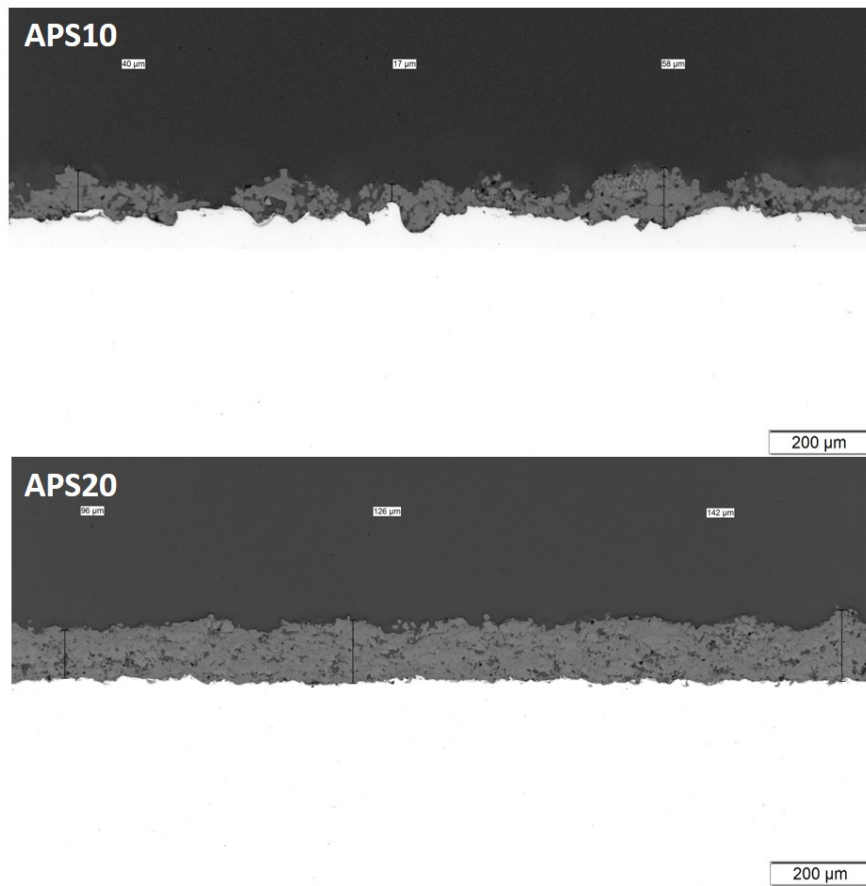


Figure 4.7: OM images of samples APS10 and APS20

Despite the APS19 higher thickness, APS22 seems to have a coating with higher density, by Figure 4.8 observation. The higher current values (600 A) of APS22 provides higher thermal energy, together with the higher amount of  $H_2$ , which results in more energy transferred to the particles. This promotes coatings with higher density and better quality, resulting from the lower amount of unmelted particles.

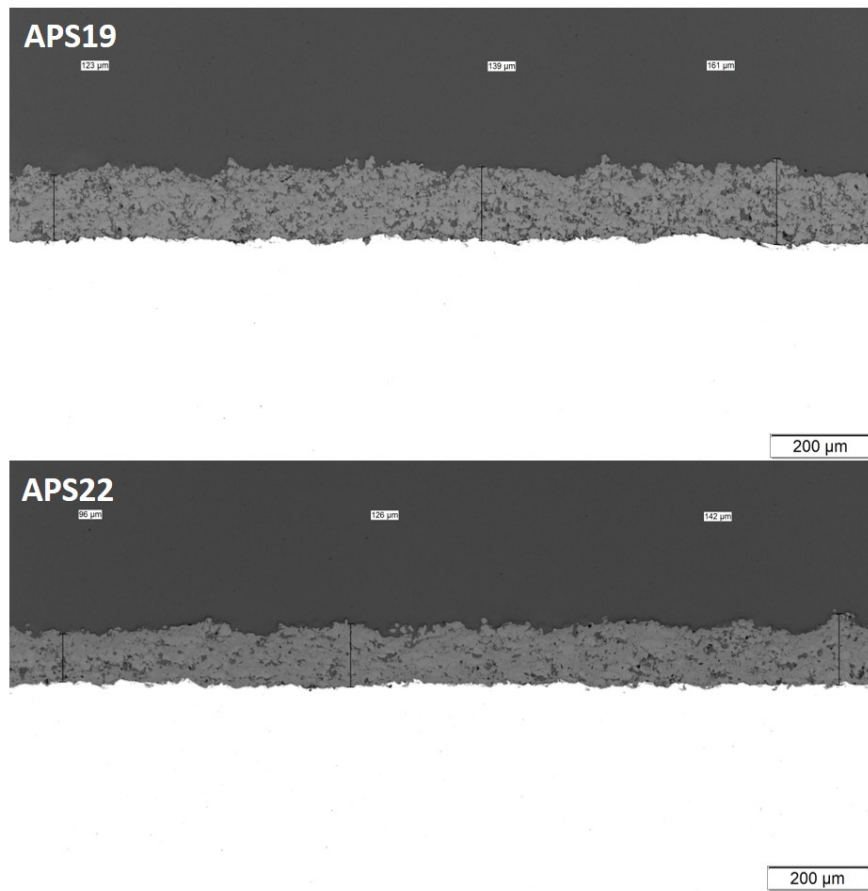


Figure 4.8: OM images of samples APS19 and APS22

However, despite the higher thermal energy of APS22, its kinetic energy is lower when compared to APS19, due to its higher spray distance (110 mm). The lower spray distance of APS19 (90 mm) prevails over its lower current to obtain thicker coatings.

#### 4.2.2 Hardness measurement

Coatings hardness depends on their porosity and cohesion between particles [133]. By analysis of Figure 4.9, APS22 higher density is the reason for its higher hardness value, when compared with APS19 and APS20. However, after the measurement of hardness at low loads, the results are inconclusive. As mentioned in the procedure, the low loads only permit the analysis of the hardness at a specific location. Thus it is not possible to uniformly analyze the coating, taking into account its porosity. When compared to the bibliography, for a load of 4 to 13 mN, ZnO reveals a hardness of around 5.0 GPa, which corresponds to approximately 510 HV [134, 135]. However, also according to literature

([136]), for the production of ZnO varistors, which are relatively porous (density of  $5.53 \pm 0.08 \text{ g/cm}^3$ ), a hardness of 2.1 GPa (214 HV) was obtained.

In this experiment, the obtained hardness values are relatively higher compared to the literature. This may be due to the splat formation, characteristic of powder APS deposition lower porosity percentage. These regions have low porosity, and, therefore, with reduced loads, it is not possible to have a complete study of the overall coating hardness.

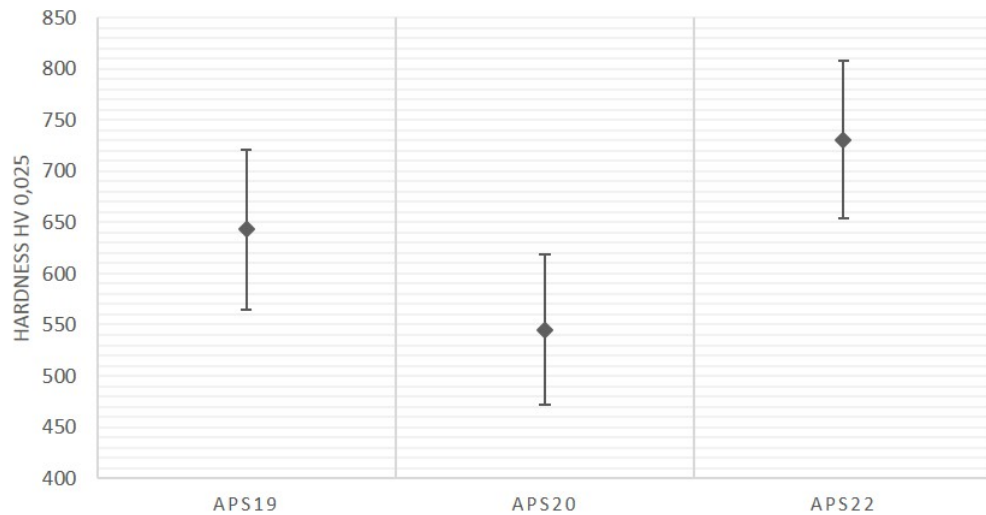


Figure 4.9: Vickers Hardness measurement of APS coatings

By analyzing the results of hardness and thickness, it can be concluded that APS22 was the best condition in relation to powder deposition. With this in consideration, APS process could be optimized. One possible approach would be the increase of the  $\text{H}_2$  which may result in a increase on the thermal energy of the sprayed particles. This can also be achieved by lowering the Ar amount, which reduces the volume of plasma interaction. Another way to achieve dense and thicker coatings, would be the decrease on the deposition rate and the increase on the number of passes. In this case the number of melted particles would be higher, and coatings with lower roughness could be obtained.

## 4.3 S-APS coating characterization

### 4.3.1 Thickness measurement

In the case of S-APS experiment, the results of the suspension deposition are displayed on Table 4.4.

Table 4.4: Suspension deposition parameters and and respective thickness measurement

Sample	Current (A)	Ar:H <sub>2</sub>	FR (ml/min)	SD (mm)	Thickness (μm)	Standard deviation
S-APS1	600	35:13	45	30	176	6
S-APS2	600	35:13	45	50	55	4
S-APS3	530	35:13	45	30	131	4
S-APS4	530	35:13	45	50	35	3
S-APS5	530	40:13	45	30	134	3
S-APS6	530	40:13	45	50	31	2
S-APS7	600	40:13	45	30	176	3
S-APS8	600	40:13	45	50	47	3

In addition to the samples of the eight experiments, the results from the center point are exhibit in Table 4.5, in order to study their linearity.

Table 4.5: Suspension deposition center point parameters and respective thickness measurement

Sample	Current (A)	Ar:H <sub>2</sub>	FR (ml/min)	SD (mm)	Thickness (μm)	μm/pass
Center Point	565	38:13	45	40	88.7	2.96

Figure 4.10 exhibit the effect of the variable spray parameters in coating thickness.

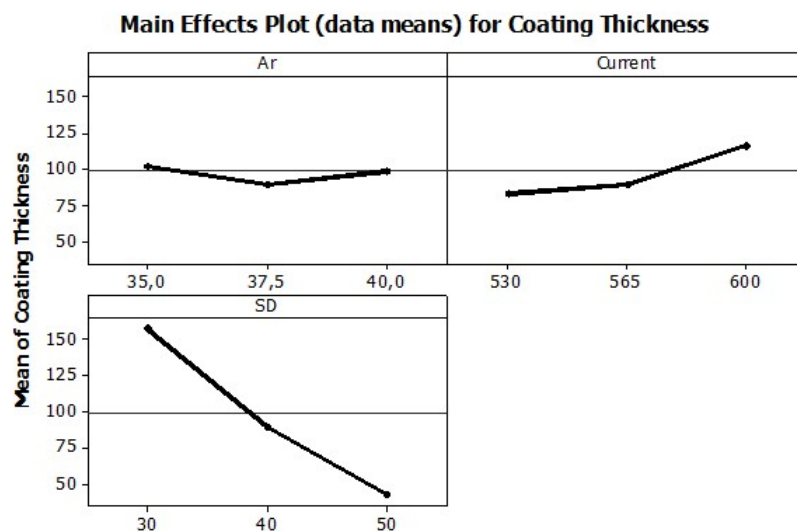


Figure 4.10: Main effect of the variable spray parameters in coating thickness

As expected, its influence was similar to the previous experiment described in 4.2. However, in S-APS experiment the spray distance was the variable with more influence,

having in consideration that the velocity loss, caused by longer distances, is more significant in smaller particles.

Observing the interaction plots of S-APS (Figure 4.11), it was concluded that variables are independent from each other, as in 4.2. However, in this experiment, the line with the most pronounced slope refers to the higher current values (green line), which has a greater effect for lower spray distances (30 mm).

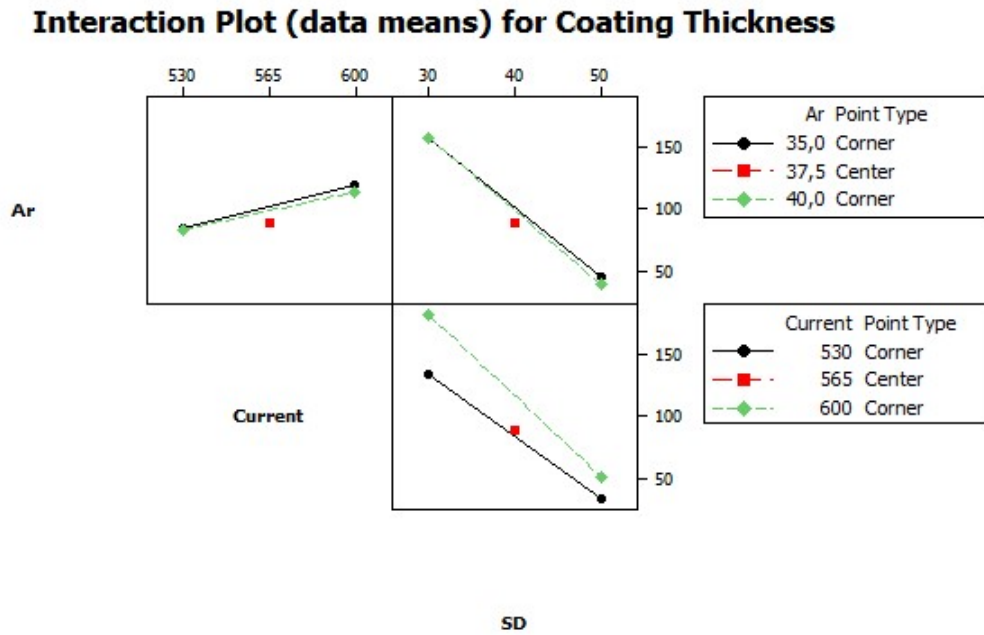


Figure 4.11: Interaction between S-APS variable spray parameters in coating thickness

Therefore, higher thicknesses were achieved for currents of 600 A. Regard to Ar:H<sub>2</sub> content, the thicker coatings, resulted from the 40:13 ratio (S-APS7). Using *Minitab*, through a Pareto chart of the effects is possible to determine the magnitude and the importance of an effect (Figure 4.12). The chart displays the absolute value of the effects (15.3). Any effect that extends beyond this reference line is potentially important, as it is the case of the current and the spray distance.

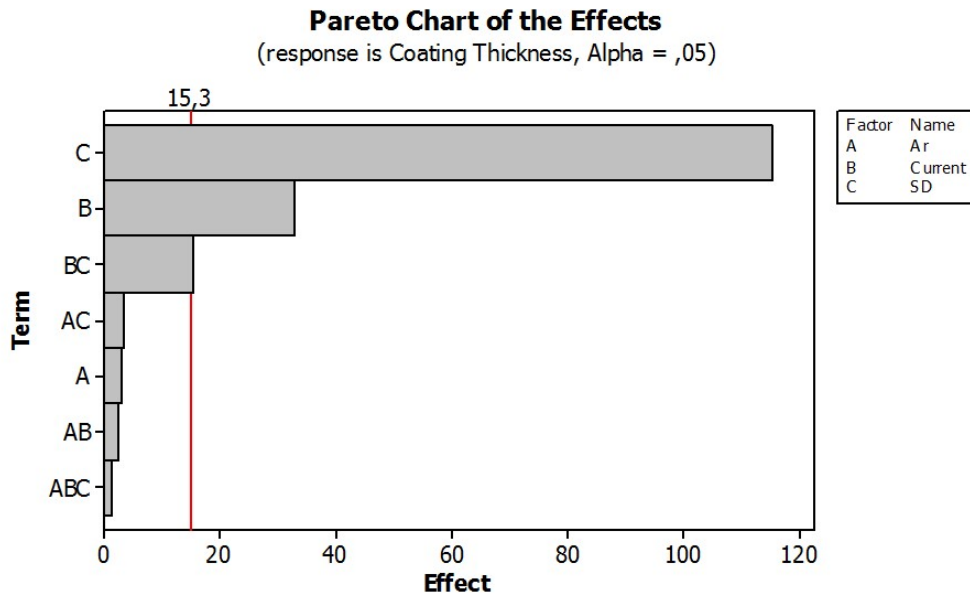


Figure 4.12: Pareto chart of effects

By the analysis of the results, presented on Table 4.4 and in Pareto chart of effects, is then conclude that the variable with the greatest impact on the coating thickness, is the spray distance (C), which has a negative effect on coating thickness. On the other hand, current (B) is the second variable with higher impact, having a positive effect in thickness results.

Regarding coating thickness, as shown in Table 4.4, the best results were achieved at the S-APS1 and S-APS7 samples (Figure 4.13).

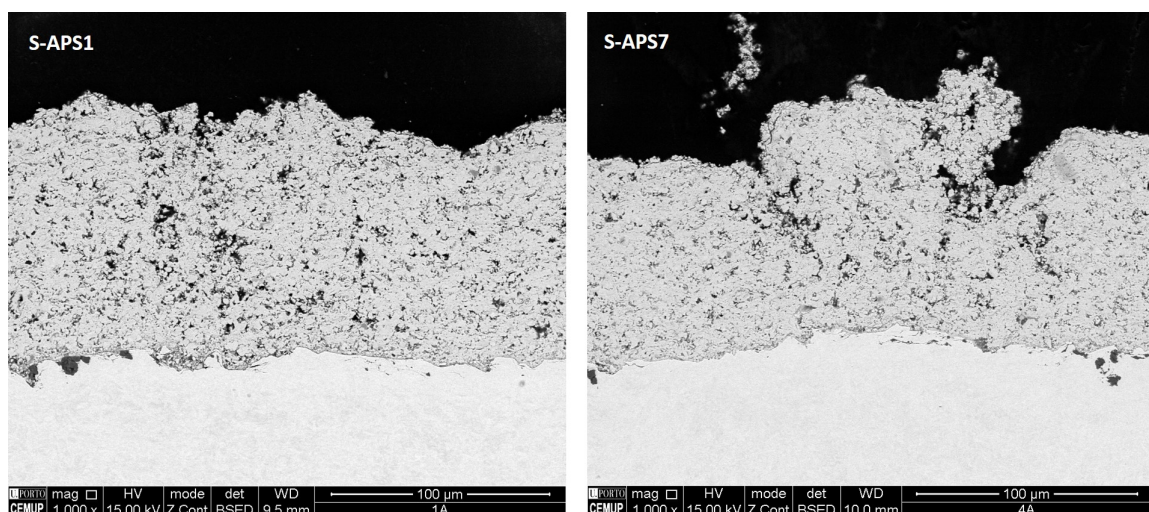


Figure 4.13: SEM images of S-APS 1 and S-APS 7 coatings

Both coatings were deposited under the same conditions, except for the content of Ar, which was higher in the S-APS7 sample (40%). As mentioned in literature ([98, 115]), Ar is responsible for the plasma formation, therefore for higher amounts, it results in a higher gas expansion. However, S-APS1 had lower Ar content (35%), which resulted in lower gas volume, and for that reason, due to the same H<sub>2</sub> content in both cases, higher thermal energy transmitted to the sprayed particles. Consequently, in S-APS1, during deposition there was more cohesion between particles which resulted in a more homogeneous coating and less surface roughness.

As for the spray distance, fewer particles reached the substrate for higher distances. For that reason, when comparing samples S-APS3 (30 mm) and S-APS4 (50 mm) (Figure 4.14), as expected, higher stand-off distances resulted in lower deposition per pass. Furthermore, the effect of gravity in the sprayed particles is superior than their velocity at the exit of the plasma gun. This results in a loss of particle's velocity, which is greater as the spray distance is increased.

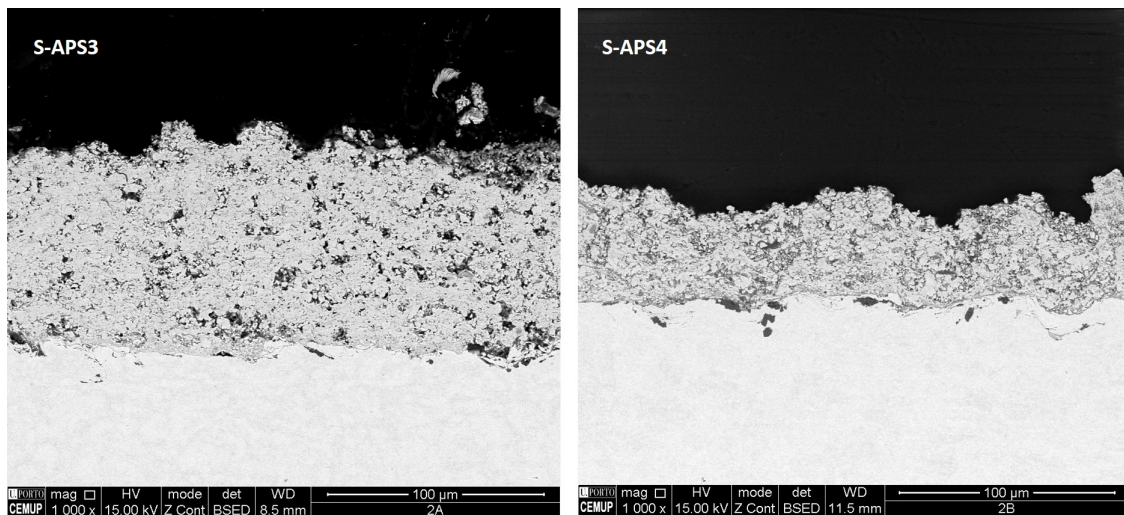


Figure 4.14: SEM images of S-APS 3 and S-APS 4 coatings

Taking the spray distance in consideration, it can be concluded that for longer distances particles have lost more thermal energy and kinetic energy. Consequently, there was a lower deposition rate in samples sprayed at 50 mm, which also resulted in lower surface roughness, as is the case of S-APS4.

In terms of the used current, by the analysis of Figure 4.13 and 4.14, it is possible to observe that the higher current of S-APS1 resulted in a positive effect on the coating thickness, comparing to S-APS3. It also appears to have lower porosity, which can be explained by higher thermal energy.

### 4.3.2 Hardness measurement

Vicker hardness results are presented in Figure 4.15. In a general way, it is concluded that the samples which were sprayed at lower distances present higher hardness values. This can be explained, as mentioned above, by the higher thermal and kinetic energy resulting from lower spray distances. This increase in energy allows a greater percentage of particles to melt, resulting in higher hardness values.

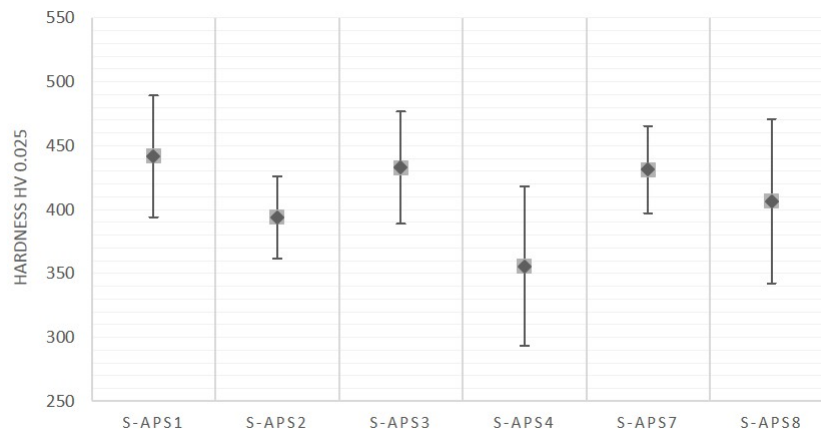


Figure 4.15: Vickers Hardness measurement of S-APS coatings

S-APS1 has a relative higher hardness value compared to the rest of the samples, as it was expected, since the higher current and lower Ar content contribute to a denser coating. For this reason, and also through the thickness results, it is possible to conclude that S-APS1 was the best condition in the case of suspension deposition. With this in mind, greater S-APS optimization can be achieved by lowering the spray distance. Furthermore, gas compositions richer in H<sub>2</sub> and with lower Ar content may also be a reasonable approach.

## 4.4 Powder vs Suspension deposition

After results analysis, APS22, S-APS1 and S-APS2 were selected for further comparison.

### 4.4.1 Coating stability in air

Al-doped ZnO feedstock material may experience degradation during APS deposition, mainly due to the recovering of the oxygen vacancies, which can be observed through coating's surface colour analysis (Figure 4.16).

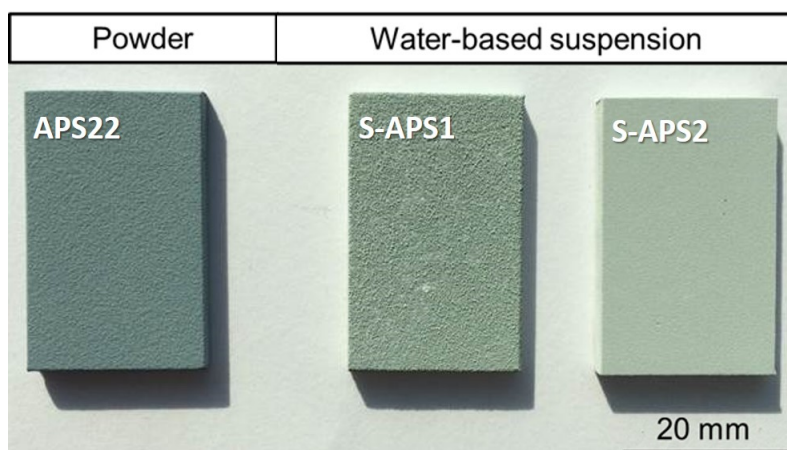


Figure 4.16: Surface image of APS22, S-APS1 and S-APS2

ZnO based materials are very sensitive to the surrounding atmospheres and can form oxygen sufficient or deficient states reversibly [21]. Its colour can change from white to yellow color when heated in air and reverting to white during cooling. This change is due to the loss of oxygen for the environment at high temperatures, in the form of non-stoichiometric  $Zn_{1+x}O$  ( $x = 0.00007$  at  $800\text{ }^{\circ}\text{C}$ ) [137]. A light green color appears due to the evaporation of a small amount of oxygen from the lattice, which results in an excess of zinc atoms, producing lattice defects that give rise to the color (yellow). On the other hand, dark greenish color mean the oxygen deficient state [21]. This colour change is visible in Figure 4.16, where APS, S-APS1 and S-APS2 sample's surface are shown. In APS20 there was a reduction, caused by the hydrogen of the plasma gas, during deposition of the coating, and thus shows a dark gray / green color. However, for the use of suspensions, due to the smaller particle size it makes it easier to react with the atmospheric oxygen and therefore has a higher oxidation rate. This is noticeable in S-APS1 and S-APS2 which show a light green/yellow colour. Although, this colour is more visible in the S-APS2 due to the greater spraying distance (50 mm), which causes the particles to be in contact with the air and higher temperatures, causing a greater oxidation of the particles, resulting in a brighter surface.

#### 4.4.2 Coating morphology

In Figure 4.17 APS22 surface's morphology is shown, in which is possible to observe the *splat* formation typical of a powder deposition by APS. There were also identified, in coating's surface, unmelted agglomerated particles. The formation of these agglomerates can be explained by the fact that, during deposition, the particles crossed the external

region of the plasma, where thermal energy is lower [133]. Moreover, the presence of some non-melted particles may also be identified on the APS22 surface.

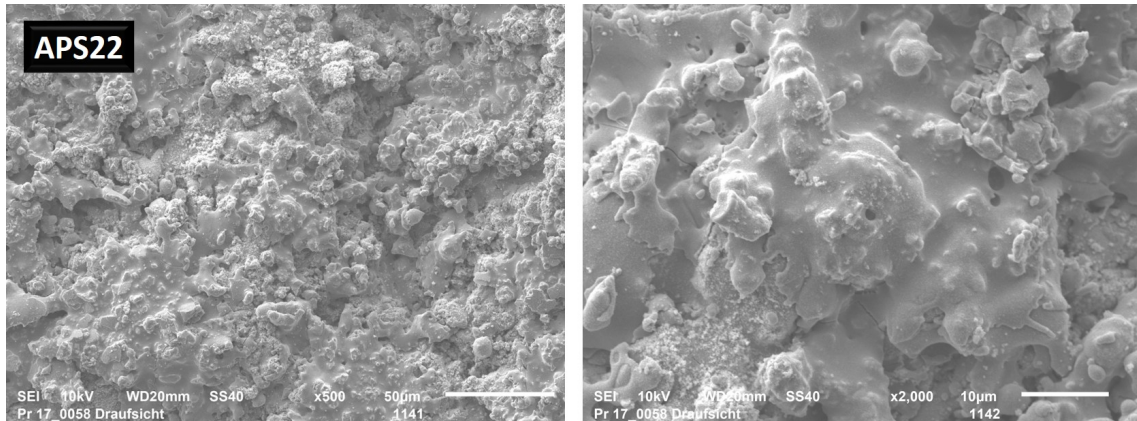


Figure 4.17: SEM images of APS22 surface

The surface morphology of S-APS1 is shown in Figure 4.18, where it is possible to observe agglomerates of nano particles of ZnO. According to the literature ([95, 138]), this morphology is denominated of cauliflower-like. Cauliflower-like formations comprised the top surfaces, could be attributed to high temperatures and rapid quenching in the plasma [95, 139]. Because to their reduced size, the particles of the suspension reach high temperatures and experience high cooling rates due to their large surface area in contact with the surrounding atmosphere. Also, the high turbulence promoted by the reduced distance of the spray may explain the formation of agglomerates. However, S-APS1's surface has high roughness and low homogeneity, due to the cauliflower-like structure.

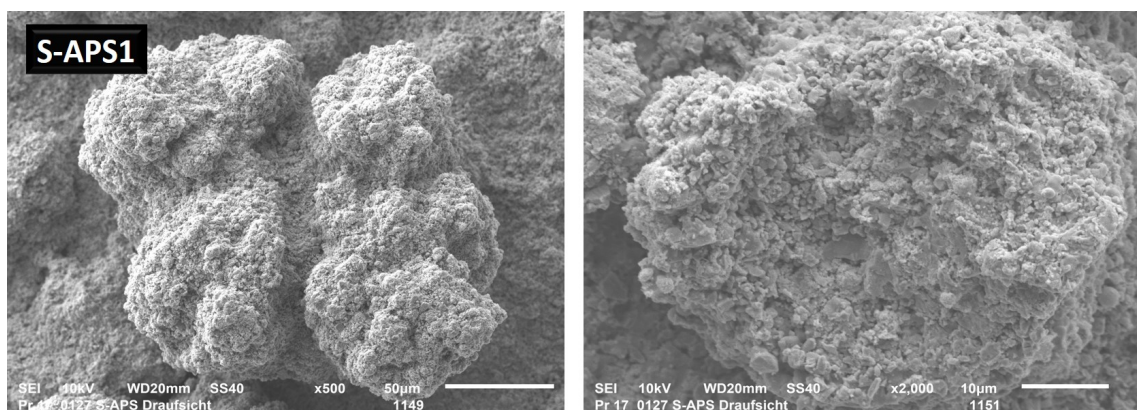


Figure 4.18: SEM images of S-APS1 surface

The cohesion between agglomerates and the other particles may be lower than in S-APS2, where a different morphology was found. Through Figure 4.19 analysis, it is possible to observe S-APS2's lower surface roughness absence of agglomerates like in the case of

S-APS1. The lower particle's velocity and lower surface temperature of S-APS2. This may be due to the higher spray distances of S-APS2, which resulted in lower particle velocity, as well as a lower surface temperature.

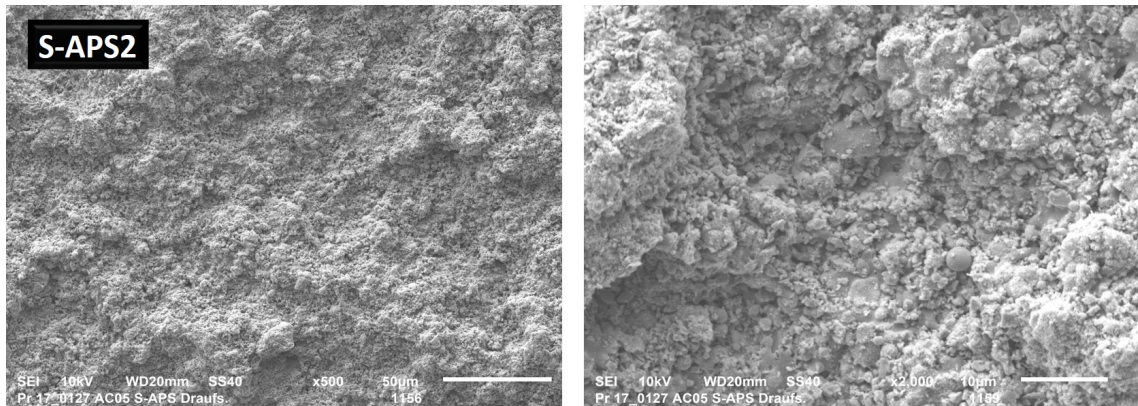


Figure 4.19: SEM images of S-APS2 surface

#### 4.4.3 Chemical composition

The resultant XRD spectra of APS22, S-APS1 and S-APS2 are shown in Figure 4.20.

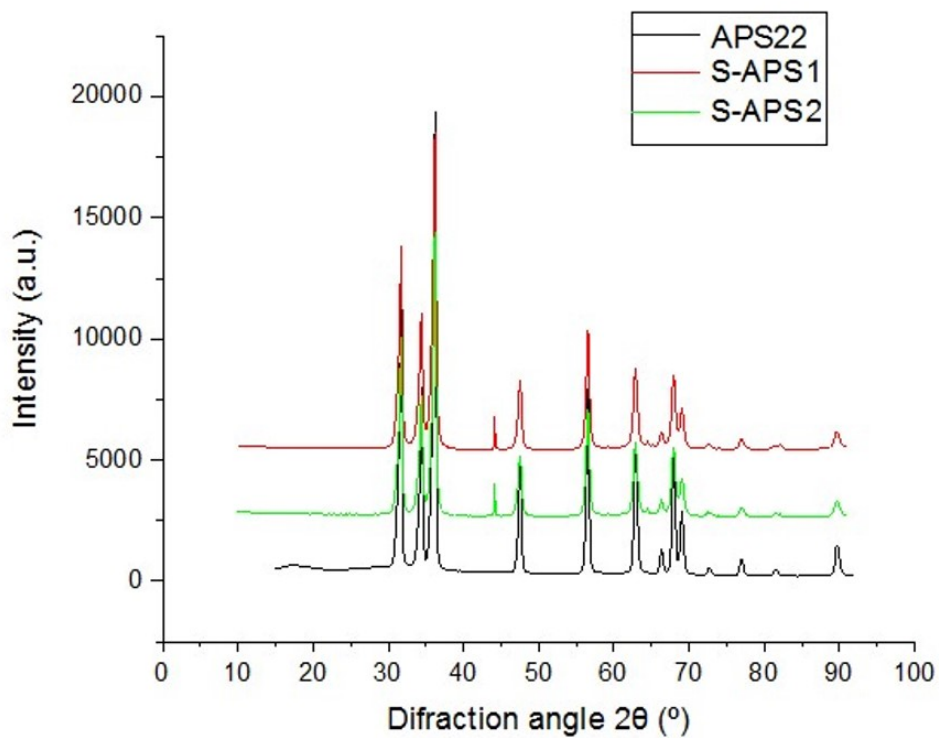


Figure 4.20: XRD analysis of APS22, S-APS1 and S-APS2 samples

The XRD spectrum (Figure 4.20) was analysed and compared with the powder diffraction files of ZnO and ZnAl<sub>2</sub>O<sub>4</sub> phases (the peaks matching is presented in Appendix 1. Through this analysis it was observed that all APS22, S-APS1 and S-APS2 have ZnO phase (PDF 00-036-1451). Furthermore, a non-identified peak ( $2\theta = 44.25^\circ$ ), was found in S-APS1 and S-APS2 spectra. This might be attributed to ZnAl<sub>2</sub>O<sub>4</sub> phase (PDF 00-005-0669), which is a product of the reaction  $\text{ZnO} + \text{Al}_2\text{O}_3 \rightarrow \text{ZnAl}_2\text{O}_4$ . This product is a result of the diffusion of Zn to Al<sub>2</sub>O<sub>3</sub>, while the Al substitution for Zn results from the diffusion of Al into ZnO [21]. However, it is possible to admit a mismatch in the resulting peaks- a phase shift. This phase shift is attributed to the non-equilibrium state of the deposited particles, which is common in APS due to the high cooling rates. Although, the presence of ZnAl<sub>2</sub>O<sub>4</sub> may also result from the higher energy transmitted to the suspension particles, which are more reactive comparing with the powder particles. This analysis is in agreement with oxidation states of S-APS1 and S-APS2 4.16.

From the point of view of thermoelectric properties, the formation of ZnAl<sub>2</sub>O<sub>4</sub> is harmful. Despite increasing the values of ZT by lowering ZnO thermal conductivity [29, 140], it can decrease thermal conductivity [29, 55].

As shown above in Figure 4.3 the feedstock material shown peaks of Zn, Al and O. Therefore, it is expected to obtain the same constituents in the EDS analysis of the final coating. Through SEM analysis, an inner coating region (Z1), was chosen for EDS analysis (Figure 4.21).

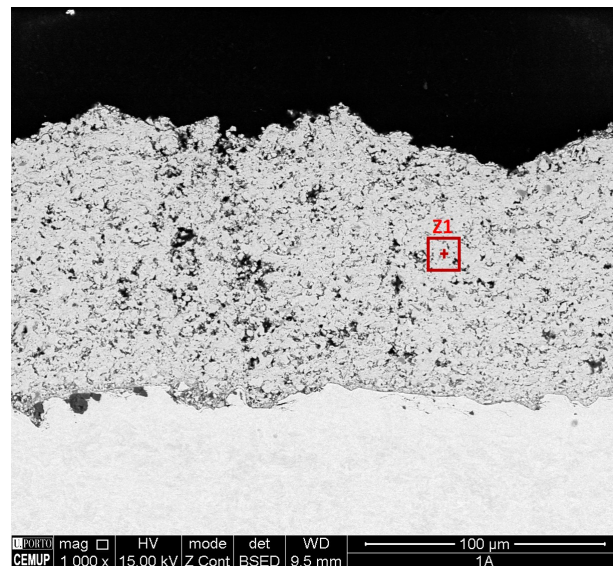


Figure 4.21: SEM images of S-APS1 cross section

Since the EDS analysis of all samples revealed similar results, only S-APS1 EDS results are presented (Figure 4.22).

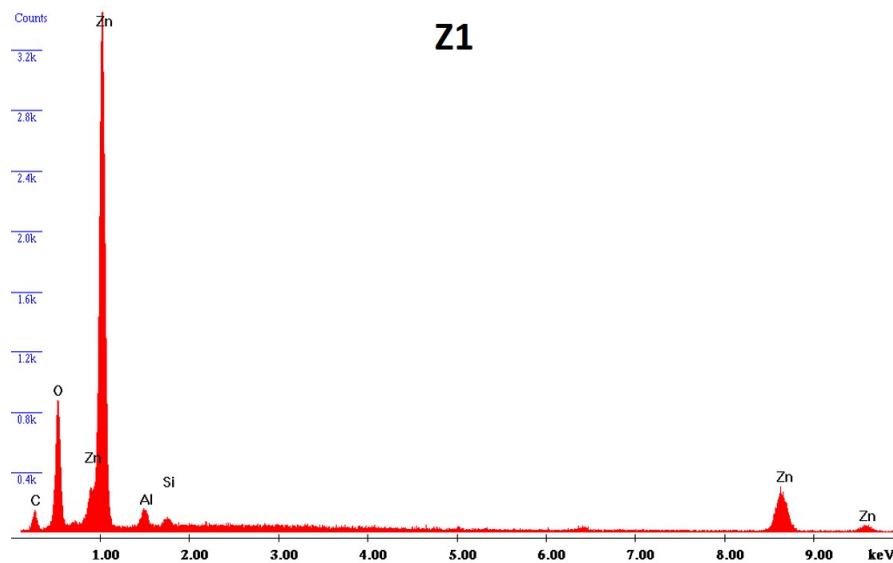


Figure 4.22: EDS spectrum of Z1 (marked in Figure 4.21)

It is then possible to observe mainly Zn (78.08 wt% ), but also O (19.34 wt%) and Al (2.58 wt% ). Additionally, a small Si peak is also shown, which is not significant, since it may result from the sample preparation, where colloidal silica was used. For this reason, it is possible that some silica content remains in the coating.

#### 4.4.4 Mechanical properties

Figure 4.23 shows the comparison between APS22 and S-APS1 hardness. For this measurement, it was used higher loads compared to the previous displayed hardness tests, in order to study the overall coating, including porosity. Although it is expected to obtain higher density for suspension deposition, when compared to powder deposition, by Figure 4.23 analysis, the hardness value is higher in APS22 than in S-APS1. This may be due to the higher content of melted particles of APS22 and the existence of microporosity in S-APS1. Despite the higher coating thickness of S-APS1 (170  $\mu\text{m}$ ) when comparing to APS22 (140  $\mu\text{m}$ ), if the cauliflower structure was removed, the resulting thickness would be significantly reduced.

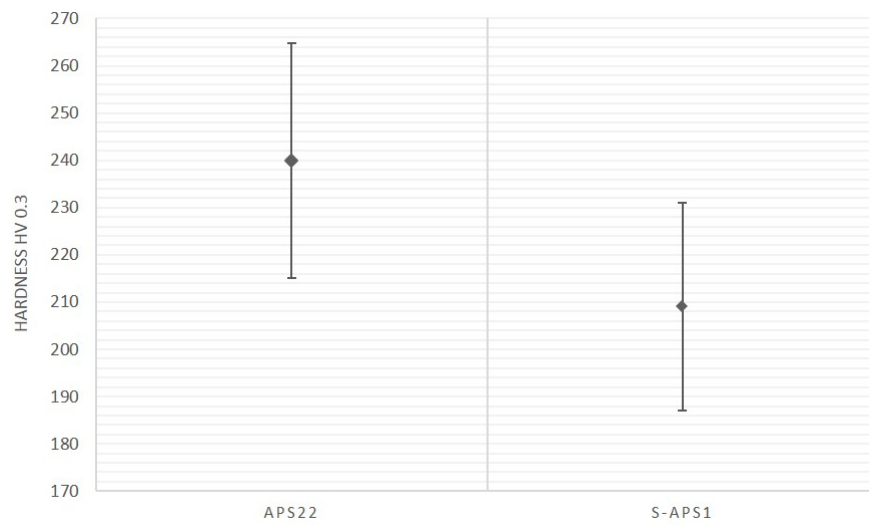


Figure 4.23: Vickers Hardness measurement (HV 0.3) of APS22 and S-APS1

As expected, by literature analysis ([98]) the results of this HV 0.3 measurement are significantly lower than those previously presented on Figure 4.9 and 4.15 with lower loads (HV 0.025). Moreover, both APS22 and S-APS1 have lower hardness than normally sinterized ZnO, due to the porosity, typical of plasma sprayed coatings [141].

# Chapter 5

## Conclusions and future work

This experiment focused on the production of dense ZnO coatings for thermoelectric applications, as is the case of thermoelectric generators. As interest in energy recovery is currently increasing, all new investigation on the subject enables the collection of new and important information. This work is not an exception since it is the first written work about APS deposition of ZnO powder and suspension.

Given the available powder, which granulometry is characterized by a  $d_{10}$  and a  $d_{90}$  of 24  $\mu\text{m}$  and 78  $\mu\text{m}$ , respectively, as well as the high melting point of ZnO, APS was the first approach as a TS process. Then, after optimizing, a new experience was performed, using a ZnO suspension, as feedstock material. However, taking into account the main goals of this work, several conclusions can be drawn:

- In APS, the parameter that influences more the coating thickness, increasing it, is the current, followed by hydrogen content. In order to obtain thicker coatings, particles should acquire large amounts of both thermal and kinetic energy. Higher current and  $\text{H}_2$  amounts provide enough thermal energy for the powder particles to successfully melt and form a coating upon impact in substrate. For this reason, in S-APS experience current was increased and  $\text{H}_2$  kept fixed in a higher value, 13 % from Ar amount.
- In S-APS, the increase of the Ar content lead to a decrease of coating thickness in both experiments. Since Ar increases plasma's volume of interaction, higher Ar percentages decreases particle's thermal energy, for the same  $\text{H}_2$  amount. In suspension deposition, after adjusting the previous used parameters, spray distance has the higher positive effect on coating thickness.

- Despite the higher coating thickness of S-APS1 (170  $\mu\text{m}$ ) when comparing to APS22 (140  $\mu\text{m}$ ), if the cauliflower structure was removed, the resulting thickness would be significantly reduced.
- Although shorter spray distances have a positive effect in the deposition rate as well as in coating thickness, the excessive kinetic energy can lead to high turbulence at the S-APS1 interface between the substrate and the coating, during deposition. This may result in coatings with high roughness and low homogeneity, in which a cauliflower-like structure is found. Therefore it is important to balance the spray distance, and increase the number of passes, in order to obtain a thicker and homogeneous coating.
- One of the main concerns in deposit ZnO is the Zn dissociation at high temperatures. In the case of the S-APS experiments, through XRD and EDS, it can be concluded that Zn remained as ZnO and reacted with the present  $\text{Al}_2\text{O}_3$  to form  $\text{ZnAl}_2\text{O}_4$ , which increases ZT by lowering the thermal conductivity. This could be a disadvantage of S-APS instead of APS. However, further tests should be made to study the influence of this phase in coating's electrical conductivity

It is then demonstrated that it is possible to successfully obtain ZnO coatings via APS. However, first is necessary to obtain even denser coatings. For that reason, further experiments should be carried out in which process parameters can be improved. One possible approach may be the increase of the  $\text{H}_2$  which may result in a increase on the thermal energy of the sprayed particles. Furthermore, by lowering the Ar amount, which reduces the volume of plasma interaction, thicker and denser coatings can be obtained. A different approach could be the reduction of the spray distance, in order to increase the amount of particles that reach the substrate.

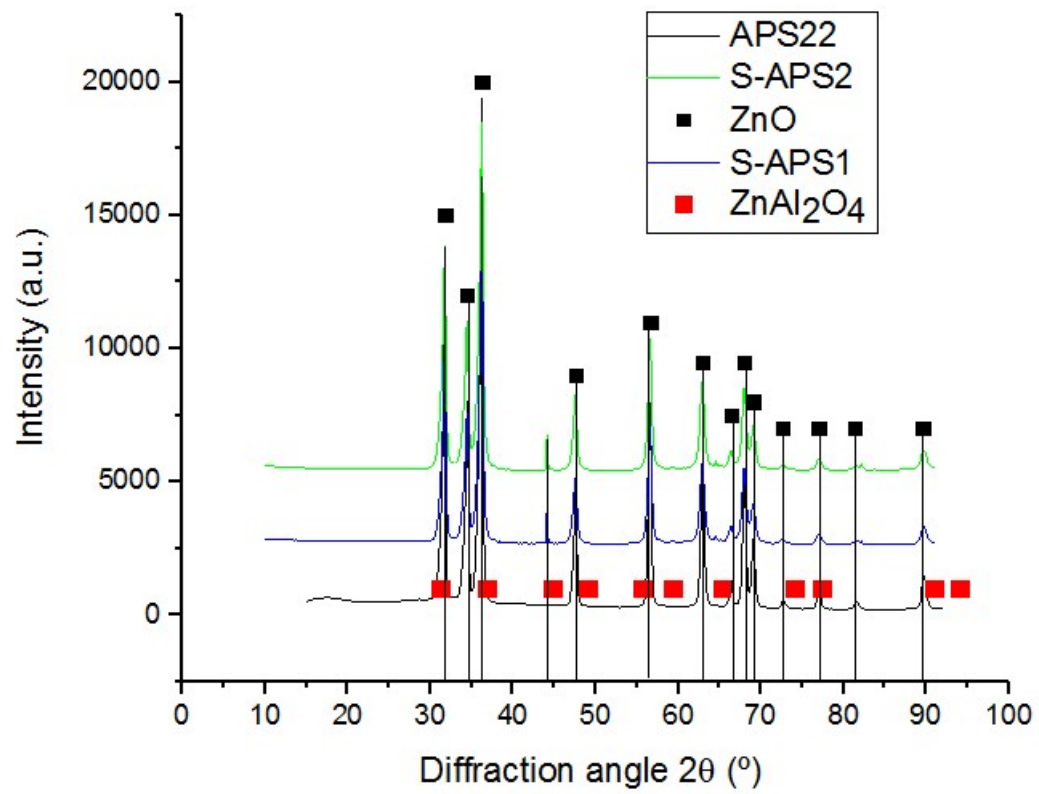
Regarding future applications, in order apply this method in thermoelectric industry, further electrical measurements are required in order to study ZnO coating's electrical properties. For example, the electrical and thermal conductivity, electrical resistivity and Seebeck coefficient, in order to calculate the Figure of Merit, ZT. However, an additional approach can be, for example, the use the same ZnO suspension in HVOF process, capable of producing coatings with very low porosity. A different approach could be the use of Ar/He gas compositions capable of achieving greater enthalpy.

Through the accomplishment of this dissertation, it can be concluded that APS is a cost-effective single step solution to deposit ZnO. In addition, APS should be further explored as a production technique of ZnO coatings, since it can bring flexibility of shape and geometry in the TE industry. After process optimization, a very important advantage

of this solution could be the production of a complete ZnO-based TEG capable of reusing energy lost in the form of heat. As global energy demand is steadily growing, awareness of global environmental preservation has also increased. Therefore the reuse of this waste heat would be one valuable approach to improve the overall energy efficiency in the different industrial sectors.

# Appendix

## 1 XRD analysis with indexed phases



# References

- [1] “Nanomaterials for energy,” <https://www.utwente.nl/mesaplus/nme/Introduction/>, Twente, Netherlands, accessed: 20/03/2017.
- [2] G. J. Snyder and E. S. Toberer, “Complex thermoelectric materials,” *Nature materials*, vol. 7, no. 2, pp. 105–114, 2008.
- [3] X. Zhang and L.-D. Zhao, “Thermoelectric materials: energy conversion between heat and electricity,” *Journal of Materiomics*, vol. 1, no. 2, pp. 92–105, 2015.
- [4] M. Barbosa, “Development of a materials concept for a large area thermally sprayed thermoelectric elements,” Ph.D. dissertation, Technische Universität Dresden, 12/08/2016.
- [5] I. Johnson, W. T. Choate, and A. Davidson, “Waste heat recovery. technology and opportunities in us industry,” BCS, Inc., Laurel, MD (United States), Tech. Rep., 2008.
- [6] T. M. Tritt and M. Subramanian, “Thermoelectric materials, phenomena, and applications: a bird’s eye view,” *MRS bulletin*, vol. 31, no. 03, pp. 188–198, 2006.
- [7] U. DOE, “Waste heat recovery: Techonology and opportunities in us industry,” *Washington DC: US Department of Energy Industrial Technologies Program*, 2008.
- [8] G. Ren, J. Lan, C. Zeng, Y. Liu, B. Zhan, S. Butt, Y.-H. Lin, and C.-W. Nan, “High performance oxides-based thermoelectric materials,” *JOM*, vol. 67, no. 1, pp. 211–221, 2015.
- [9] P. L. Fauchais, J. V. Heberlein, and M. I. Boulos, “Wire arc spraying,” in *Thermal Spray Fundamentals*. Springer, 2014, pp. 577–629.
- [10] K. Schackenberg, E. Muller, J. Schilz, W. Kaysser, G. Langer, and E. Lugscheider, “Ageing properties of thermally sprayed iron disilicide,” in *Thermoelectrics, 1997. Proceedings ICT’97. XVI International Conference on*. IEEE, 1997, pp. 307–310.
- [11] G. Langer, *Verarbeitbarkeit thermoelektrischer Materialien durch Plasmaspritzverfahren*. Mainz, 2001.
- [12] J. Schilz, M. Riffel, R. Mathesius, G. Schiller, R. Henne, and R. W. Smith, “Plasma spray forming as a novel production method for thermoelectric materials,” in *Thermoelectrics, 1996., Fifteenth International Conference on*. IEEE, 1996, pp. 71–74.
- [13] J. Schilz, E. Müller, K. Schackenberg, H. Ernst, W. Kaysser, G. Langer *et al.*, “On the thermoelectric performance of plasma spray–formed iron disilicide,” *Journal of materials science letters*, vol. 17, no. 17, pp. 1487–1490, 1998.
- [14] E. Lugscheider and G. Langer, “Thermal spraying of fgms for thermoelectric devices,” in *Materials science forum*, vol. 308. Trans Tech Publ, 1999, pp. 748–753.

- [15] K. Ueno, S. Sodeoka, M. Suzuki, A. Tsutsumi, K. Kuramoto, J. Sawazaki, K. Yoshida, H. Huang, K. Nagai, H. Kondo *et al.*, “Fabrication of large size FeSi/sub 2/thermoelectric device by thermal spraying process,” in *Thermoelectrics, 1998. Proceedings ICT 98. XVII International Conference on.* IEEE, 1998, pp. 418–421.
- [16] S. Sodeoka, M. Suzuki, T. Inoue, and J. Rückriem, “Thermoelectric device fabricated by plasma spray,” in *Proc. of the 2007 Int. Thermal Spray Conf., B. Marple (Ed.), Published by ASM International, Beijing, People’s Republic of China, 2007*, pp. 313–318.
- [17] S. Sodeoka, M. Suzuki, T. Inoue, and H. Obara, “Thermoelectric properties of plasma sprayed (Sr, Y) TiO<sub>x</sub> thick film,” in *Proc. of 2008 Int. Thermal Spray Conf., E. Lugscheider (Ed.), Maastricht, The Netherlands, 2008*.
- [18] J. P. Longtin, L. Zuo, D. Hwang, G. Fu, M. Tewolde, Y. Chen, and S. Sampath, “Fabrication of thermoelectric devices using thermal spray: application to vehicle exhaust systems,” *Journal of thermal spray technology*, vol. 22, no. 5, pp. 577–587, 2013.
- [19] J. W. Fergus, “Oxide materials for high temperature thermoelectric energy conversion,” *Journal of the European Ceramic Society*, vol. 32, no. 3, pp. 525–540, 2012.
- [20] A. Janotti and C. G. Van de Walle, “Fundamentals of zinc oxide as a semiconductor,” *Reports on progress in physics*, vol. 72, no. 12, p. 126501, 2009.
- [21] L. Han, “High temperature thermoelectric properties of ZnO based materials,” Ph.D. dissertation, 2014.
- [22] A. Kołodziejczak-Radzimska and T. Jesionowski, “Zinc oxide—from synthesis to application: a review,” *Materials*, vol. 7, no. 4, pp. 2833–2881, 2014.
- [23] K. Cai, E. Müller, C. Drašar, and A. Mrotzek, “Preparation and thermoelectric properties of Al-doped ZnO ceramics,” *Materials Science and Engineering: B*, vol. 104, no. 1, pp. 45–48, 2003.
- [24] X. Liang, “Structure and thermoelectric properties of ZnO based materials,” Ph.D. dissertation, 2013.
- [25] “Thermoelectric materials,” <http://cmc.chem.au.dk/research/energy-materials/thermoelectrics/>, accessed: 24/03/2017.
- [26] G. S. Nolas, J. Sharp, and J. Goldsmid, *Thermoelectrics: basic principles and new materials developments.* Springer Science & Business Media, 2013, vol. 45.
- [27] H. E. Katz and T. O. Poehler, *Innovative Thermoelectric Materials: Polymer, Nanostructure and Composite Thermoelectrics.* World Scientific, 2016.
- [28] G. J. Snyder and T. S. Ursell, “Thermoelectric efficiency and compatibility,” *Physical review letters*, vol. 91, no. 14, p. 148301, 2003.
- [29] T. Tsubota, M. Ohtaki, K. Eguchi, and H. Arai, “Thermoelectric properties of al-doped ZnO as a promising oxidematerial for high-temperature thermoelectric conversion,” *Journal of Materials Chemistry*, vol. 7, no. 1, pp. 85–90, 1997.
- [30] B. E. White, “Energy-harvesting devices: Beyond the battery,” *Nature nanotechnology*, vol. 3, no. 2, pp. 71–72, 2008.
- [31] D. S. Lashmore, M. White, B. White, D. Degtiarov, and J. Mann, “Nanostructured material-based thermoelectric generators,” Aug. 14 2008, uS Patent App. 12/191,765.
- [32] D. M. Rowe, *CRC handbook of thermoelectrics.* CRC press, 1995.

- [33] G. J. Snyder, T. Caillat, and J.-P. Fleurial, "Thermoelectric, transport, and magnetic properties of the polaron semiconductor  $\text{Fe}_x\text{Cr}_3\text{Se}_4$ ," *Physical Review B*, vol. 62, no. 15, p. 10185, 2000.
- [34] A. F. Ioffe, L. Stil'bans, E. Iordanishvili, T. Stavitskaya, A. Gelbtuch, and G. Vineyard, "Semiconductor thermoelements and thermoelectric cooling," *Physics Today*, vol. 12, p. 42, 1959.
- [35] J. Dong, W. Liu, H. Li, X. Su, X. Tang, and C. Uher, "In situ synthesis and thermoelectric properties of PbTe-graphene nanocomposites by utilizing a facile and novel wet chemical method," *Journal of Materials Chemistry A*, vol. 1, no. 40, pp. 12 503–12 511, 2013.
- [36] "Lehrstuhl für experimentalphysik iv," <https://www.physik.uni-augsburg.de/exp4/Research/Thermoelectric-Materials/>, Augsburg, Germany, accessed: 27/03/2017.
- [37] R. G. Morris, R. Redin, and G. Danielson, "Semiconducting properties of  $\text{Mg}_2\text{Si}$  single crystals," *Physical Review*, vol. 109, no. 6, p. 1909, 1958.
- [38] R. D. Redin, R. Morris, and G. Danielson, "Semiconducting properties of  $\text{Mg}_2\text{Ge}$  single crystals," *Physical Review*, vol. 109, no. 6, p. 1916, 1958.
- [39] D. Rowe, J. Smith, G. Thomas, and G. Min, "Weight penalty incurred in thermoelectric recovery of automobile exhaust heat," *Journal of electronic materials*, vol. 40, no. 5, pp. 784–788, 2011.
- [40] J.-i. Tani and H. Kido, "Thermoelectric properties of Bi-doped  $\text{Mg}_2\text{Si}$  semiconductors," *Physica B: Condensed Matter*, vol. 364, no. 1, pp. 218–224, 2005.
- [41] V. Zaitsev, M. Fedorov, E. Gurieva, I. Eremin, P. Konstantinov, A. Y. Samunin, and M. Vedernikov, "Highly effective  $\text{Mg}_2\text{Si}_x\text{Sn}_x$  thermoelectrics," *Physical Review B*, vol. 74, no. 4, p. 045207, 2006.
- [42] J. Tervo, A. Manninen, R. Ilola, and H. Hänninen, "State-of-the-art of thermoelectric materials processing," *VTT Technical Research Center of Finland, Vuorimiehentie*, 2009.
- [43] C. C. Sorrell, J. Nowotny, and S. Sugihara, *Materials for energy conversion devices*. Elsevier, 2005.
- [44] S. LeBlanc, S. K. Yee, M. L. Scullin, C. Dames, and K. E. Goodson, "Material and manufacturing cost considerations for thermoelectrics," *Renewable and Sustainable Energy Reviews*, vol. 32, pp. 313–327, 2014.
- [45] G. Kieslich, G. Cerretti, I. Veremchuk, R. P. Hermann, M. Panthöfer, J. Grin, and W. Tremel, "A chemists view: Metal oxides with adaptive structures for thermoelectric applications," *physica status solidi (a)*, 2016.
- [46] T. Talebi, R. Ghomashchi, P. Talemi, and S. Aminorroaya, "Electrophoretic deposition of p-type  $\text{Bi}_2\text{Te}_3$  for thermoelectric applications," *World Academy of Science, Engineering and Technology, International Journal of Chemical, Molecular, Nuclear, Materials and Metallurgical Engineering*, vol. 11, no. 4, pp. 253–256, 2017.
- [47] B. Hall, "Powder processing, powder characterization, and mechanical properties of last (lead-antimony-silver-tellurium) and lastt (leadantimony-silver-tellurium-tin) thermoelectric materials," *Unpublished Master's Thesis, Michigan State University*, 2008.
- [48] N. Tsujii, J. H. Roudebush, A. Zevalkink, C. A. Cox-Uvarov, G. J. Snyder, and S. M. Kauzlarich, "Phase stability and chemical composition dependence of the thermoelectric properties of the type-i clathrate  $\text{Ba}_8\text{Al}_x\text{Si}_{46-x}$ ," *Journal of Solid State Chemistry*, vol. 184, no. 5, pp. 1293–1303, 2011.
- [49] J. H. Roudebush, N. Tsujii, A. Hurtando, H. Hope, Y. Grin, and S. M. Kauzlarich, "Phase range of the type-i clathrate  $\text{Sr}_8\text{Al}_x\text{Si}_{46}$  and crystal structure of  $\text{Sr}_8\text{Al}_{10}\text{Si}_{36}$ ," *Inorganic chemistry*, vol. 51, no. 7, pp. 4161–4169, 2012.

- [50] H. U. Kessel, J. Hennicke, J. Schmidt, T. Weißgräber, B. F. Kieback, M. Herrmann, and J. Räthel, "Feldaktives sintern „fast“ –ein neues verfahren zur herstellung metallischer und keramischer sinterwerkstoffe," in *Hagener Symposium*, 2006.
- [51] H. Boettner, D. Ebling, A. Jacquot, U. Kühn, and J. Schmidt, "Melt spinning preparation of bismuth telluride and partially alloying with iv-vi compounds for thermoelectric application," in *MRS Proceedings*, vol. 1044. Cambridge Univ Press, 2007, pp. 1044–U04.
- [52] G. Tan, W. Liu, S. Wang, Y. Yan, H. Li, X. Tang, and C. Uher, "Rapid preparation of  $\text{CeFe}_4\text{Sb}_{12}$  skutterudite by melt spinning: rich nanostructures and high thermoelectric performance," *Journal of Materials Chemistry A*, vol. 1, no. 40, pp. 12 657–12 668, 2013.
- [53] K. Simunovic, "Thermal spraying," *Encyclopedia of Life Support Systems, Welding Engineering and Technology*, 2010.
- [54] H. Böttner, D. G. Ebling, A. Jacquot, J. König, L. Kirste, and J. Schmidt, "Structural and mechanical properties of spark plasma sintered n-and p-type bismuth telluride alloys," *physica status solidi (RRL)-Rapid Research Letters*, vol. 1, no. 6, pp. 235–237, 2007.
- [55] P. Jood, R. J. Mehta, Y. Zhang, G. Peleckis, X. Wang, R. W. Siegel, T. Borca-Tasciuc, S. X. Dou, and G. Ramanath, "Al-doped zinc oxide nanocomposites with enhanced thermoelectric properties," *Nano letters*, vol. 11, no. 10, pp. 4337–4342, 2011.
- [56] D. Gautam, M. Engenhorst, C. Schilling, G. Schierning, R. Schmechel, and M. Winterer, "Thermoelectric properties of pulsed current sintered nanocrystalline al-doped ZnO by chemical vapour synthesis," *Journal of Materials Chemistry A*, vol. 3, no. 1, pp. 189–197, 2015.
- [57] J. Wang, J. Cao, B. Fang, P. Lu, S. Deng, and H. Wang, "Synthesis and characterization of multipod, flower-like, and shuttle-like ZnO frameworks in ionic liquids," *Materials Letters*, vol. 59, no. 11, pp. 1405–1408, 2005.
- [58] Z. L. Wang, "Splendid one-dimensional nanostructures of zinc oxide: a new nanomaterial family for nanotechnology," *Acs Nano*, vol. 2, no. 10, pp. 1987–1992, 2008.
- [59] R. Könenkamp, R. Word, and M. Godinez, "Ultraviolet electroluminescence from ZnO/polymer heterojunction light-emitting diodes," *Nano Letters*, vol. 5, no. 10, pp. 2005–2008, 2005.
- [60] M.-C. Jeong, B.-Y. Oh, M.-H. Ham, and J.-M. Myoung, "Electroluminescence from ZnO nanowires in n-zn o film/ZnO nanowire array/p-ga n film heterojunction light-emitting diodes," *Applied Physics Letters*, vol. 88, no. 20, p. 202105, 2006.
- [61] M. A. Zimmler, T. Voss, C. Ronning, and F. Capasso, "Exciton-related electroluminescence from ZnO nanowire light-emitting diodes," *Applied Physics Letters*, vol. 94, no. 24, p. 241120, 2009.
- [62] B. Ludi and M. Niederberger, "Zinc oxide nanoparticles: chemical mechanisms and classical and non-classical crystallization," *Dalton Transactions*, vol. 42, no. 35, pp. 12 554–12 568, 2013.
- [63] Ü. Özgür, Y. I. Alivov, C. Liu, A. Teke, M. Reshchikov, S. Doğan, V. Avrutin, S.-J. Cho, and H. Morkoc, "A comprehensive review of ZnO materials and devices," *Journal of applied physics*, vol. 98, no. 4, p. 11, 2005.
- [64] S. Bhattacharyya and A. Gedanken, "A template-free, sonochemical route to porous ZnO nanodisks," *Microporous and Mesoporous Materials*, vol. 110, no. 2, pp. 553–559, 2008.
- [65] M. Chaari and A. Matoussi, "Electrical conduction and dielectric studies of ZnO pellets," *Physica B: Condensed Matter*, vol. 407, no. 17, pp. 3441–3447, 2012.

- [66] Z. L. Wang, "Splendid one-dimensional nanostructures of zinc oxide: a new nanomaterial family for nanotechnology," *Acs Nano*, vol. 2, no. 10, pp. 1987–1992, 2008.
- [67] S. Adachi, "Polarization and wave-vector-dependent measurements by four-wave mixing in ZnO: valence-band ordering and biexcitons," *Journal of luminescence*, vol. 112, no. 1, pp. 34–39, 2005.
- [68] T. Tian, L. Cheng, L. Zheng, J. Xing, H. Gu, S. Bernik, H. Zeng, W. Ruan, K. Zhao, and G. Li, "Defect engineering for a markedly increased electrical conductivity and power factor in doped ZnO ceramic," *Acta Materialia*, vol. 119, pp. 136–144, 2016.
- [69] N. L. Marana, J. R. Sambrano, and A. R. d. Souza, "Propriedades eletrônicas, estruturais e constantes elásticas do ZnO," *Química Nova*, pp. 810–815, 2010.
- [70] J. Lim, C. Yeoh, P. Teh, A. Chik, and W. Arif, "Effect of Al doping concentration to the physical and thermoelectric properties of zinc oxide," *Australian Journal of Basic and Applied Sciences*, vol. 7, no. 5, pp. 21–25, 2013.
- [71] H. Cheng, X. Xu, H. Hng, and J. Ma, "Characterization of Al-doped ZnO thermoelectric materials prepared by rf plasma powder processing and hot press sintering," *Ceramics International*, vol. 35, no. 8, pp. 3067–3072, 2009.
- [72] N. Ma, J.-F. Li, B. Zhang, Y. Lin, L. Ren, and G. Chen, "Microstructure and thermoelectric properties of  $Zn_{1-x}Al_xO$  ceramics fabricated by spark plasma sintering," *Journal of Physics and Chemistry of Solids*, vol. 71, no. 9, pp. 1344–1349, 2010.
- [73] K. Shirouzu, T. Ohkusa, M. Hotta, and N. Enomoto, "Distribution and solubility limit of Al in  $Al_2O_3$ -doped ZnO sintered body," *Journal of the Ceramic Society of Japan*, vol. 115, no. 1340, pp. 254–258, 2007.
- [74] J. Y. Seto, "The electrical properties of polycrystalline silicon films," *Journal of Applied Physics*, vol. 46, no. 12, pp. 5247–5254, 1975.
- [75] T. K. Gupta and W. G. Carlson, "A grain-boundary defect model for instability/stability of a ZnO varistor," *Journal of materials science*, vol. 20, no. 10, pp. 3487–3500, 1985.
- [76] H. Takemoto, K. Fugane, P. Yan, J. Drennan, M. Saito, T. Mori, and H. Yamamura, "Reduction of thermal conductivity in dually doped ZnO by design of three-dimensional stacking faults," *RSC Advances*, vol. 4, no. 6, pp. 2661–2672, 2014.
- [77] D. Thomas, "Interstitial zinc in zinc oxide," *Journal of Physics and Chemistry of Solids*, vol. 3, no. 3-4, pp. 229–237, 1957.
- [78] G. W. Tomlins, J. L. Routbort, and T. O. Mason, "Zinc self-diffusion, electrical properties, and defect structure of undoped, single crystal zinc oxide," *Journal of applied physics*, vol. 87, no. 1, pp. 117–123, 2000.
- [79] L. Schmidt-Mende and J. L. MacManus-Driscoll, "ZnO-nanostructures, defects, and devices," *Materials today*, vol. 10, no. 5, pp. 40–48, 2007.
- [80] J. Liu, F. Xiu, L. Mandalapu, and Z. Yang, "P-type ZnO by Sb doping for pn-junction photodetectors," in *Integrated Optoelectronic Devices 2006*. International Society for Optics and Photonics, 2006, pp. 61 220H–61 220H.
- [81] C. G. Van de Walle, "Hydrogen as a cause of doping in zinc oxide," *Physical review letters*, vol. 85, no. 5, p. 1012, 2000.
- [82] J. Bian, X. Li, C. Zhang, W. Yu, and X. Gao, "p-type ZnO films by monodoping of nitrogen and ZnO-based p–n homojunctions," *Applied Physics Letters*, vol. 85, no. 18, pp. 4070–4072, 2004.

- [83] M. Ohtaki, T. Tsubota, K. Eguchi, and H. Arai, "Thermoelectric performance of ZnO-based mixed oxides as a promising high-temperature material," in *Proc. 14th Int. Conf. Thermoelectrics*, 1995, pp. 245–248.
- [84] M. Ohtaki, "Oxide thermoelectric materials for heat-to-electricity direct energy conversion," 2009.
- [85] K. H. Kim, S. H. Shim, K. B. Shim, K. Niihara, and J. Hojo, "Microstructural and thermoelectric characteristics of zinc oxide-based thermoelectric materials fabricated using a spark plasma sintering process," *Journal of the American Ceramic Society*, vol. 88, no. 3, pp. 628–632, 2005.
- [86] M. Omori and T. Hirai, "Fabrication of functional gradient materials by spark plasma sintering," *New Ceram. Japan*, vol. 7, pp. 4–8, 1994.
- [87] Z. Shen, M. Johnsson, Z. Zhao, and M. Nygren, "Spark plasma sintering of alumina," *Journal of the American Ceramic Society*, vol. 85, no. 8, pp. 1921–1927, 2002.
- [88] C. L. Wu, L. Chang, H. G. Chen, C. W. Lin, Y. C. Chao, J. K. Yan *et al.*, "Growth and characterization of chemical-vapor-deposited zinc oxide nanorods," *Thin Solid Films*, vol. 498, no. 1, pp. 137–141, 2006.
- [89] T. Polley and W. Carter, "Zone model for zinc oxide deposited by combustion chemical vapor deposition," *Thin Solid Films*, vol. 384, no. 2, pp. 177–184, 2001.
- [90] A. Fiddes, K. Durose, A. Brinkman, J. Woods, P. Coates, and A. Banister, "Preparation of ZnO films by spray pyrolysis," *Journal of crystal growth*, vol. 159, no. 1-4, pp. 210–213, 1996.
- [91] M. Krunk, T. Dedova, and I. O. Açıık, "Spray pyrolysis deposition of zinc oxide nanostructured layers," *Thin Solid Films*, vol. 515, no. 3, pp. 1157–1160, 2006.
- [92] A. George, P. Kumari, N. Soin, S. Roy, and J. McLaughlin, "Microstructure and field emission characteristics of ZnO nanoneedles grown by physical vapor deposition," *Materials Chemistry and Physics*, vol. 123, no. 2, pp. 634–638, 2010.
- [93] M. Ohyama, H. Kouzuka, and T. Yoko, "Sol-gel preparation of ZnO films with extremely preferred orientation along (002) plane from zinc acetate solution," *Thin solid films*, vol. 306, no. 1, pp. 78–85, 1997.
- [94] M. Kamalasanan and S. Chandra, "Sol-gel synthesis of ZnO thin films," *Thin Solid Films*, vol. 288, no. 1-2, pp. 112–115, 1996.
- [95] R. Tummala, R. K. Guduru, and P. S. Mohanty, "Solution precursor plasma deposition of nanostructured ZnO coatings," *Materials Research Bulletin*, vol. 46, no. 8, pp. 1276–1282, 2011.
- [96] C. Ghosh, S. Das, and K. Chattopadhyay, "Enhancement of thermopower of Mn doped ZnO thin film," *Physica B: Condensed Matter*, vol. 399, no. 1, pp. 38–46, 2007.
- [97] M. Tului, A. Bellucci, A. Albolino, and G. Migliozi, "Zinc oxide targets for magnetron sputtering pvd prepared by plasma spray," *Surface and Coatings Technology*, vol. 205, no. 4, pp. 1070–1073, 2010.
- [98] L. Pawlowski, *The science and engineering of thermal spray coatings*. John Wiley & Sons, 2008.
- [99] M. R. Dorfman, "Thermal spray coatings," *Handbook of Environmental Degradation of Materials*. Norwich, NY: William Andrew Publishing, pp. 405–422, 2005.
- [100] T. J. Levingstone, "Optimisation of plasma sprayed hydroxyapatite coatings," Ph.D. dissertation, Dublin City University, 2008.

- [101] J. R. Davis *et al.*, *Handbook of thermal spray technology*. ASM international, 2004.
- [102] G. Queirós, “Ceramic based wear resistant coatings via thermal spray,” *Faculdade de Engenharia da Universidade do Porto*, 2017.
- [103] H. Herman and S. Sampath, “Thermal spray coatings,” in *Metallurgical and ceramic protective coatings*. Springer, 1996, pp. 261–289.
- [104] L.-M. Berger, “Application of hardmetals as thermal spray coatings,” *International Journal of Refractory Metals and Hard Materials*, vol. 49, pp. 350–364, 2015.
- [105] A. Ghabchi, *Wear resistant carbide-based thermal sprayed coatings: process, properties, mechanical degradation and wear*, 2011.
- [106] A. Wank, “Basics of thermal spray technology i processes,” *GTV Verschleiss-Schutz GmbH*.
- [107] M. Roy, *Thermal Sprayed Coatings and Their Tribological Performances*. IGI Global, 2015.
- [108] “An introduction to thermal spray,” <https://www.oerlikon.com/metco/en/products-services/coating-equipment/thermal-spray/>, accessed: 30/03/2017.
- [109] D. Matejka and B. Benko, “Plasma spraying of metallic and ceramic materials,” *John Wiley and Sons, Baffins Lane, Chichester, West Sussex, PO 19 1 UD, UK, 1989. 280*, 1989.
- [110] J. C. Tan, “Optimisation of the hvof thermal spray process for coating, forming and repair of components,” Ph.D. dissertation, Dublin City University, 1997.
- [111] T. Stoltenhoff, H. Kreye, and H. Richter, “An analysis of the cold spray process and its coatings,” *Journal of Thermal Spray Technology*, vol. 11, no. 4, pp. 542–550, 2002.
- [112] S. Kuroda, J. Kawakita, M. Watanabe, and H. Katanoda, “Warm spraying—a novel coating process based on high-velocity impact of solid particles,” *Science and technology of advanced materials*, vol. 9, no. 3, p. 033002, 2008.
- [113] M. Jadidi, M. Mousavi, S. Moghtadernejad, and A. Dolatabadi, “A three-dimensional analysis of the suspension plasma spray impinging on a flat substrate,” *Journal of Thermal Spray Technology*, vol. 24, no. 1-2, pp. 11–23, 2015.
- [114] M. Jadidi, S. Moghtadernejad, and A. Dolatabadi, “A comprehensive review on fluid dynamics and transport of suspension/liquid droplets and particles in high-velocity oxygen-fuel (hvof) thermal spray,” *Coatings*, vol. 5, no. 4, pp. 576–645, 2015.
- [115] H.-A. Mathesius and W. Krömmer, *Praxis des thermischen Spritzens: Anleitung für das Fachpersonal*. DVS Media, 2009.
- [116] L. Pawlowski, “Suspension and solution thermal spray coatings,” *Surface and Coatings Technology*, vol. 203, no. 19, pp. 2807–2829, 2009.
- [117] R. Vaßen, H. Kaßner, G. Mauer, and D. Stöver, “Suspension plasma spraying: process characteristics and applications,” *Journal of Thermal Spray Technology*, vol. 19, no. 1-2, pp. 219–225, 2010.
- [118] F.-L. Toma, “Suspension thermal spraying: An industrial breakthrough for thermal spraying,” *Fraunhofer-Institut für Werkstoffund Strahltechnik IWS*.
- [119] “Suspension thermal spraying - hardware components for industrial use,” Fraunhofer IWS, Dresden, Germany, Tech. Rep.
- [120] “Suspension thermal spraying - an industrial breakthrough for thermal spraying,” Fraunhofer IWS, Dresden, Germany, Tech. Rep.

- [121] F.-L. Toma, A. Potthoff, L.-M. Berger, and C. Leyens, "Demands, potentials, and economic aspects of thermal spraying with suspensions: A critical review," *Journal of Thermal Spray Technology*, vol. 24, no. 7, pp. 1143–1152, 2015.
- [122] A. Killinger, R. Gadow, G. Mauer, A. Guignard, R. Vaßen, and D. Stöver, "Review of new developments in suspension and solution precursor thermal spray processes," *Journal of Thermal Spray Technology*, vol. 20, no. 4, p. 677, 2011.
- [123] "Progressive surface: Thermal spray," [http://www.progressivesurface.com/faqs\\_thermalspraying.htm](http://www.progressivesurface.com/faqs_thermalspraying.htm), Michigan, USA, accessed: 31/03/2017.
- [124] A. P. Filofteia-Laura Toma, Christoph Leyens, "Demands, potentials and economic aspects of thermal spraying with aqueous suspensions," in *Thermal Spray of Suspensions and Solutions Symposium (TS4)*, Montreal, Canada, F. IWS and F. IKTS, Eds., Dec. 2015.
- [125] M. Barbosa, R. Kratzsch, P. Annegret, O. Kunze, N. Kulissa, and T. Filofteia-Laura, "Development and application of binary suspensions in the ternary system  $\text{Cr}_2\text{O}_3\text{-TiO}_2\text{-Al}_2\text{O}_3$  for s-hvof spraying," *Fraunhofer IKTS, Fraunhofer IWS and Technische Universität Dresden*, 2017.
- [126] F.-L. Toma, C. Stahr, L.-M. Berger, S. Saaro, M. Herrmann, D. Deska, and G. Michael, "Corrosion resistance of APS-and HVOF-sprayed coatings in the  $\text{Al}_2\text{O}_3\text{-TiO}_2$  system," *Journal of thermal spray technology*, vol. 19, no. 1-2, pp. 137–147, 2010.
- [127] R. U. S. M. Madelung, O., Ed., *Zinc oxide (ZnO) Debye temperature, heat capacity, density, melting point, vapor pressure, hardness*. Berlin, Heidelberg: Springer Berlin Heidelberg, 1999, pp. 1–5. [Online]. Available: [http://dx.doi.org/10.1007/10681719\\_312](http://dx.doi.org/10.1007/10681719_312)
- [128] M. Shamsuddin, *Physical chemistry of metallurgical processes*. John Wiley & Sons, 2016.
- [129] J. N. Miller and J. C. Miller, *Statistics and chemometrics for analytical chemistry*. Pearson Education, 2005.
- [130] "Interpret the key results for interaction plot," <http://support.minitab.com/en-us/minitab-express/1/help-and-how-to/modeling-statistics/anova/how-to/interaction-plot/interpret-the-results/>, accessed: 28/05/2017.
- [131] "Fischer technology," <http://www.fischer-technology.com/en/united-states/>, Windsor, USA, accessed: 01/06/2017.
- [132] D. C. Zipperian, "Metallographic specimen preparation basics," *Pace Technologies. Disponível em* <http://www.metallographic.com/Basics.htm>. Acesso em Agosto, 2006.
- [133] S. Deng, H. Liao, C. Zeng, and C. Coddet, "Thermal spray 2006: building on 100 years of success," in *Proceedings of 2006 International Thermal Spray Conference, ASM International, Materials Park, Ohio, USA (May 15–18, 2006)*, 2006, p. 1437.
- [134] I. Yonenaga, "Thermo-mechanical stability of wide-bandgap semiconductors: high temperature hardness of SiC, AlN, GaN, ZnO and ZnSe," *Physica B: Condensed Matter*, vol. 308, pp. 1150–1152, 2001.
- [135] S. Kucheyev, J. Bradby, J. Williams, C. Jagadish, and M. Swain, "Mechanical deformation of single-crystal ZnO," *Applied Physics Letters*, vol. 80, no. 6, pp. 956–958, 2002.
- [136] H. Yoshimura, A. L. Molisani, N. Narita, J. Manholetti, and J. Cavenaghi, "Mechanical properties and microstructure of zinc oxide varistor ceramics," in *Materials science forum*, vol. 530. Trans Tech Publ, 2006, pp. 408–413.

- [137] E. Wiberg and N. Wiberg, *Inorganic Chemistry*. Academic Press, 2001. [Online]. Available: <https://books.google.pt/books?id=Mtth5g59dEIC>
- [138] T. Gordon, J. Grinblat, and S. Margel, "Preparation of "cauliflower-like" ZnO micron-sized particles," *Materials*, vol. 6, no. 11, pp. 5234–5246, 2013.
- [139] M. Tului, F. Arezzo, and L. Pawlowski, "Optical properties of plasma sprayed ZnO + Al<sub>2</sub>O<sub>3</sub> coatings," *Surface and Coatings Technology*, vol. 179, no. 1, pp. 47–55, 2004.
- [140] N. Ma, J.-F. Li, B. Zhang, Y. Lin, L. Ren, and G. Chen, "Microstructure and thermoelectric properties of Zn<sub>1-x</sub>Al<sub>x</sub>O ceramics fabricated by spark plasma sintering," *Journal of Physics and Chemistry of Solids*, vol. 71, no. 9, pp. 1344–1349, 2010.
- [141] A. Mukhopadhyay, M. Ray Chaudhuri, A. Seal, S. Dalui, M. Banerjee, and K. Phani, "Mechanical characterization of microwave sintered zinc oxide," *Bulletin of Materials Science*, vol. 24, no. 2, pp. 125–128, 2001.